Formation of a distinctive complex between the inducible bacterial lysine decarboxylase and a novel AAA+ ATPase

Jamie Snider, Irina Gutsche, Michelle Lin, Sabulal Baby, Brian Cox, Gareth Butland, Jack Greenblatt, Andrew Emili, Walid A. Houry

THE JOURNAL OF BIOLOGICAL CHEMISTRY VOL. 281, NO. 3, pp. 1532–1546, January 20, 2006

Formation of a Distinctive Complex between the Inducible Bacterial Lysine Decarboxylase and a Novel AAA+ ATPase*

Received for publication, October 13, 2005 Published, JBC Papers in Press, November 21, 2005, DOI 10.1074/jbc.M511172200

Jamie Snider[‡1], Irina Gutsche[§2], Michelle Lin[‡], Sabulal Baby[‡], Brian Cox[¶], Gareth Butland[‖], Jack Greenblatt[‖3], Andrew Emili[‖3], and Walid A. Houry[‡4]

From the [‡]Department of Biochemistry, University of Toronto, Toronto, Ontario M5S 1A8, Canada, the [¶]Samuel Lunenfeld Research Institute, Mount Sinai Hospital and Department of Medical Genetics and Microbiology, University of Toronto, Toronto, Ontario M5S 1A8, Canada, the [‖]Banting and Best Department of Medical Research and Department of Medical Genetics and Microbiology, University of Toronto, Toronto, Ontario M5S 1A8, Canada, and the [§]Laboratoire de Virologie Moléculaire et Structurale, UMR 2472/1157, CNRS-Institut National de la Recherche Agronomique and Institut Fédératif de Recherche 115, 1 Avenue de la Terrasse, 91198 Gif-sur-Yvette Cedex, France

AAA+ ATPases are ubiquitous proteins that employ the energy obtained from ATP hydrolysis to remodel proteins, DNA, or RNA. The MoxR family of AAA+ proteins is widespread throughout bacteria and archaea but is largely uncharacterized. Limited work with specific members has suggested a potential role as molecular chaperones involved in the assembly of protein complexes. As part of an effort aimed at determining the function of novel AAA+ chaperones in *Escherichia coli*, we report the characterization of a representative member of the MoxR family, YieN, which we have renamed RavA (regulatory ATPase variant A). We show that the *ravA* gene exists on an operon with another gene encoding a protein, YieM, of unknown function containing a Von Willebrand Factor Type A domain. RavA expression is under the control of the σ^S transcription factor, and its levels increase toward late log/early stationary phase, consistent with its possible role as a general stress-response protein. RavA functions as an ATPase and forms hexameric oligomers. Importantly, we demonstrate that RavA interacts strongly with inducible lysine decarboxylase (LdcI or CadA) forming a large cage-like structure consisting of two LdcI decamers linked by a maximum of five RavA oligomers. Surprisingly, the activity of LdcI does not appear to be affected by binding to RavA in a number of *in vitro* and *in vivo* assays, however, complex formation results in the stimulation of RavA ATPase activity. Data obtained suggest that the RavA-LdcI interaction may be important for the regulation of RavA activity against its targets.

The AAA+ (ATPases associated with various cellular activities) superfamily of proteins comprises a large and functionally diverse class of P-loop NTPases. Members of this superfamily are involved in a wide range of cellular processes, including protein refolding/degradation, transcriptional regulation, ribosome and organelle biogenesis, DNA repair and replication, and molecular transport events (1, 2). Proteins belonging to this superfamily contain one or more copies of the AAA+ module, which is a 200- to 250-amino acid region containing several distinct conserved motifs (1, 3, 4), including the Walker A and Walker B consensus sequences. AAA+ modules are responsible for ATP binding and hydrolysis, the energy of which is then harnessed for use in molecular rearrangement events (5). AAA+ proteins oligomerize, typically forming ring-shaped hexamers (6).

Recent phylogenetic analyses using sequence and structural information have identified numerous families of AAA+ proteins (1, 2, 7, 8). One major but poorly characterized family is the MoxR family, which is widespread throughout bacteria and archaea, with members being represented in all major lineages (1, 2, 8). The exact functional role of MoxR proteins is unclear, although limited work with members of this family suggests a chaperone-like role in the assembly/activation of specific protein complexes. The first characterized member of this family is MoxR in *Paracoccus denitrificans*, which was shown to be important in the biogenesis of methanol dehydrogenase. Cells in which the *moxR* gene was disrupted produced wild-type levels of methanol dehydrogenase, but, surprisingly, the enzyme was not functional (9). Another MoxR-related protein, NorQ/NirQ, was shown to be important in the biogenesis of nitric-oxide reductase. As with MoxR and methanol dehydrogenase, disruptions of the *norQ/nirQ* gene resulted in the production of non-functional nitric-oxide reductase enzyme in *Pseudomonas stutzeri*, *P. denitrificans*, and *Rhodobacter sphaeroides* (10–12). Also, the CbbQ gene product, a MoxR-related protein, was shown to alter Rubisco[4] conformation and stimulate its activity upon overexpression of recombinant forms of the proteins together in an *Escherichia coli* system (13, 14). Yet another MoxR family member, GvpN, has been shown to be important in gas vesicle biogenesis in certain organisms (15–18). The exact role and mechanism of function of MoxR proteins in all of these processes are not clear.

Genes encoding MoxR proteins frequently co-occur in close proximity to genes encoding proteins containing Von Willebrand Factor Type A (VWA) domains, suggesting that these gene products may be functionally linked. For example, the MoxR family members, *norQ* and *cbbQ* genes, are encoded on the same operon as, and immediately upstream of, the *norD* and *cbbO* genes, respectively, which encode VWA proteins.

* This work was supported in part by a grant from the Natural Sciences and Engineering Research Council of Canada (to W. A. H.). The costs of publication of this article were defrayed in part by the payment of page charges. This article must therefore be hereby marked "*advertisement*" in accordance with 18 U.S.C. Section 1734 solely to indicate this fact.

[1] Recipient of a graduate fellowship from the Natural Sciences and Engineering Research Council of Canada.

[2] To whom questions regarding EM methodology should be addressed: IVMS, c/o EMBL Grenoble Outstation 38042 Grenoble Cedex 9, France. E-mail: gutsche@embl-grenoble.fr.

[3] Supported by the Ontario Genomics Institute and Genome Canada.

[4] A Canadian Institutes of Health Research New Investigator. To whom correspondence should be addressed: 1 King's College Circle, Medical Sciences Bldg., Dept. of Biochemistry, University of Toronto, Toronto, Ontario M5S 1A8, Canada. Tel.: 416-946-7141; Fax: 416-978-8548; E-mail: walid.houry@utoronto.ca.

[4] The abbreviations used are: Rubisco, ribulose-bisphosphate carboxylase/oxygenase; VWA, Von Willebrand Factor Type A; LdcI, inducible lysine decarboxylase; DTT, dithiothreitol; MES, 4-morpholineethanesulfonic acid; TAPS, 3-{[2-hydroxy-1,1-bis(hydroxymethyl)ethyl]amino}-1-propanesulfonic acid; BSA, bovine serum albumin; WT, wild-type; PLP, pyridoxal phosphate; TNBS, 2,4,6-trinitrobenzenesulfonic acid; RT, reverse transcription; EM, electron microscopy; ATP-γS, adenosine 5′-*O*-(thiotriphosphate); ORF, open reading frame; FTC, fraction three complex.

Both NorD and CbbO were shown to be important in the activation of functional nitric-oxide reductase and Rubisco, respectively (11–13). The VWA domain is a metal-binding domain often mediating protein-protein interactions (19). The metal is typically magnesium. Metal-binding occurs through a non-contiguous metal ion-dependent adhesion site, which is important for binding protein ligands (20). VWA proteins have been well studied in eukaryotes, where they are involved in a range of processes, including cell adhesion, transport, the complement system, proteolysis, transcription, DNA repair, and ribosome biogenesis. Bacterial and archaeal VWA proteins are not as well characterized, although limited work has identified members involved in surface adhesion, serum opacity, fibrinogen binding, and metal insertion into protoporphyrin IX (21–23). Thus, to carry out their varied remodeling functions, many MoxR AAA+ proteins probably work in conjunction with VWA domain-containing proteins.

As part of a research project aimed at identifying novel AAA+ chaperones in *E. coli*, we became interested in the uncharacterized protein YieN (SwissProt number P31473), which defines a MoxR subfamily (2). We have renamed this protein RavA (regulatory ATPase variant A). Here, we show that RavA is a cytoplasmic, hexameric AAA+ protein that functions with a VWA domain-containing protein, YieM (SwissProt number P03818), which we termed ViaA (VWA interacting with AAA+ ATPase). Detailed information is presented on RavA gene organization, expression patterns, protein subcellular localization, enzymatic activity, and oligomerization properties. Furthermore, we show that RavA strongly interacts with the inducible lysine decarboxylase (LdcI or CadA, SwissProt number P0A9H3), an enzyme important in bacterial acid stress response, to form a distinctive 5-fold symmetric cage-like complex as determined by electron microscopy.

MATERIALS AND METHODS

Bioinformatics—A total of 156 proteins belonging to the MoxR AAA+ family, as defined by the Clusters of Orthologous Groups (MoxR COG0714), were selected for analysis (24). These sequences included those currently identified in the COG data base as belonging to COG0714, as well as additional sequences extracted using the BLASTP program from 427 microbial genomes in the NCBI sequence data base (25). All additional sequences were analyzed using the COGNITOR program to ensure that they belonged to COG0714 (26). A multiple sequence alignment was then constructed using the ClustalW program (27). The phylogenetic tree was generated using the PROTDIST and FITCH programs included in the PHYLIP package (28). A PMB model of substitution (29) and global rearrangement were used. Default settings were used for all other parameters.

36 sequences identified as belonging to the RavA subfamily of MoxR AAA+ were selected and aligned using ClustalW. This alignment was then used to identify residues conserved in >90% of sequences. Conservation was based upon the following amino acid groupings: ILVM, KR, DE, ST, YFW, and NQ. Ungrouped amino acids included Ala, Cys, Pro, His, and Gly.

Bacterial Strains—Wild-type MG1655 strain was purchased from ATCC (ATCC Number 47076). MG1655 Δ*ravA* strain was constructed from WT MG1655 using the Lambda Red system as described (30, 31). Briefly, knock-out cassette containing the chloramphenicol resistance marker was amplified by PCR from pKD3 plasmid using primers RKO-_forward (5′-agaaacgtctatactcgcaatttacgcagaacttttgacgaaagggtgtaggctggagctgcttc-3′) and RKO_reverse (5′-aatctgtgcaccgacatcctgtaggctggcttcaatgcgacctaacatatgaatatcctccttag-3′) to construct the *ravA* deletion strain, or VKO_forward (5′-ctgaaggcggcaatcactgatgatgttccccgctggcgtgaaggtgtaggctggagctgcttc-3′) and VKO_reverse (5′-gcgagagcgtcccttctctgctgtaataatttatcgccgccagcgcatatgaatatcctcctcttag-3′) to construct the *viaA* (*yieM_ECOLI*) deletion strain. DY330 cells were inoculated from single colonies into 50 ml of LB media and grown at 30 °C with shaking to $A_{600} = 0.6 – 0.8$. 25 ml of culture was heated in a 42 °C water bath with shaking for 15 min to induce expression of the Lambda Red genes *exo*, *bet*, and *gam*. Cells were immediately cooled on ice for 10 min. Cells were made electrocompetent and then transformed with 1–2 μl of linear PCR product using a Bio-Rad GenePulser. Transformed cells were diluted into 1 ml of LB and grown at 30 °C for 1 h. Cells were then plated onto LB agar containing 25 μg/ml chloramphenicol and grown overnight at 30 °C. Resistant colonies were selected and screened for successful deletion of the gene(s) using PCR. The deletion cassette was then transferred from DY330 to MG1655 using P1Δ*dam rev6* transduction as described previously (32). Verification of the deletion strains was performed using PCR, DNA sequencing, and Northern and Western blot analyses. It should be noted that deletion of *ravA* resulted in a strain that also cannot transcribe *viaA* (see Fig. 4, *A* and *B*).

The RavA-TAP-encoding strain was constructed using the Lambda Red system in a manner similar to that described for the construction of the knock-out strains. Specific details on strain construction, as well as on the pull-down and identification of bands by mass spectrometry, are provided elsewhere (33). MG1655 Δ*rpoS* and Δ*cadB* strains were obtained from the *E. coli* genome project at the University of Wisconsin, Madison, WI.

Gene Cloning—ravA (*yieN_ECOLI*), *ldcI* (*cadA*/*dcly*_ECOLI), and *ldcC* (*dclz*_ECOLI) genes were cloned from *E. coli* K12 MG1655, whereas *viaA* was cloned from *E. coli* O157:H7. It should be noted that the amino acid sequences of ViaA from *E. coli* K12 MG1655 and O157:H7 strains are identical. Primers used were as follows: RAVA_forward (5′-atcacgatcatatggctcaccctcatttattag-3′), RAVA_reverse (5′-tacgtaggatccttagcattgttgtgcctggcg-3′), VIAA_forward (5′-aactcgatcatatgctaacgctggatacg-3′), VIAA_reverse (5′-ctatggatccttatcgccgccagcgtctgagc-3′), LDCI_forward (5′-atgctaccatatgaacgttattgcaatattg-3′), LDCI_reverse (5′-ctggatccttatttcttgctttcttctttcaatacc-3′), LDCC_forward (5′-tctaccatgggcatgaacatcattgccattatg-3′), and LDCC_reverse (5′-cacctcgagttatcccgccatttttaggac-3′).

ravA was cloned into p11 plasmid (34), a modified pET15b, which adds His_6 followed by a tobacco etch virus-cut site to the N terminus of the expressed protein (HV tag). *viaA* and *ldcI* were cloned into pET3a (Novagen), which expresses untagged proteins. *ldcC* was cloned into pET16b such that it was expressed untagged, with the exception of additional N-terminal Gly and Met residues. All constructs were verified by DNA sequencing.

Protein Expression and Purification—Proteins were expressed in BL21(DE3) pLysS (Stratagene). RavA, ViaA, and LdcI protein expression was induced by addition of 0.4 mM isopropyl 1-thio-β-D-galactopyranoside to cultures grown to midlog phase. Cultures expressing RavA were grown overnight at 30 °C in the presence of inducer, and those expressing ViaA were induced at 18 °C overnight. Cultures expressing LdcI were induced for 3 h at 37 °C. LdcC cultures were grown at 37 °C for 24 h without the addition of isopropyl 1-thio-β-D-galactopyranoside. Following induction, cells were harvested by centrifugation at 3000 × *g* for 20 min and stored at −80 °C pending purification.

RavA was purified using Qiagen nickel-nitrilotriacetic acid-agarose beads according to the manufacturer's protocols. The HV tag was removed by digestion with tobacco etch virus protease at 1:10 molar ratio of tobacco etch virus to protein for 5 h at 4 °C. The protein was further purified using a Mono S HR 5/5 column.

ViaA was precipitated from cell lysate using 30% ammonium sulfate. Pellets were resuspended and exchanged into a no-salt buffer using

PD10 desalting columns. The protein was further purified on a Heparin HP5 column.

Cells overexpressing LdcI were lysed in buffer LI1 (25 mM Tris-HCl, pH 7.5, 300 mM NaCl, 0.1 mM pyridoxal 5′-phosphate, 5% glycerol, and 1 mM DTT). Cell debris was removed by centrifugation. The supernatant was heated at 70 °C for 5 min resulting in the precipitation of the bulk of *E. coli* proteins, however, most of LdcI remained soluble. Precipitate was removed by centrifugation at 30,000 × *g* for 15 min. LdcI in the supernatant was further purified by ion exchange chromatography using a Mono Q HR 5/5 column and then by size exclusion chromatography using a Superdex 200 HR 10/30 column.

LdcC was precipitated from cell lysate using 30% ammonium sulfate, and the pellets were resuspended and exchanged into low salt buffer by dialysis. The protein was further purified using a Mono Q HR 5/5 column.

The final yields of purified proteins per 1 liter of culture were as follows: 6 mg for RavA, 2 mg for ViaA, 10 mg for LdcI, and 5 mg for LdcC. Proteins were judged to be >95% pure by SDS-PAGE analysis. All chromatography columns used were from Amersham Biosciences. Protein concentration was determined using the Bio-Rad Protein Assay.

Measurement of RavA ATPase Activity—RavA ATPase activity was measured by determining the free phosphate released after ATP hydrolysis using a colorimetric assay similar to that reported previously (35). Briefly, RavA was placed in buffer RA1 (5 mM $MgCl_2$, 0.02% Triton X-100, and 1 mM DTT) containing various concentrations of ATP substrate. RA1 solutions of different pH were generated using 10 mM concentrations of citrate, acetate, MES, HEPES, or TAPS buffers. Where applicable, BSA, ViaA, LdcI, and LdcC were included in the buffer. Assays were performed in 100-μl volumes at 37 °C in Eppendorf tubes or in a quartz plate. At different time points, 10-μl aliquots of the assay mixture were removed and added to 200 μl of RA2 (1 mM malachite green, 8.5 mM ammonium molybdate, and 1 M HCl). Color development was allowed to proceed for 1 min and then was stopped by the addition of 25 μl of 37% citric acid. Absorbance was measured at 660 nm and converted to moles of phosphate produced using a KH_2PO_4 standard curve.

Preparation of Cell Extracts for LdcI Activity Assays—WT and Δ*ravA* cells were grown in LB media containing 0.4% glucose to an A_{600} of 3.0–4.0 at 37 °C. Cells were pelleted by centrifugation, resuspended in lysis buffer LT1 (25 mM HEPES, pH 7.0, 300 mM NaCl, 10% glycerol, and 5 mM β-mercaptoethanol), and lysed by sonication. The lysates were cleared of debris by centrifugation, flash frozen on liquid N_2, and stored at −80 °C until use in assays.

Measurement of LdcI Lysine Decarboxylase Activity—The ability of LdcI to generate cadaverine from lysine was measured as previously described with slight modification (36). Purified LdcI was dissolved in buffer LA1 (2.5 mM $MgCl_2$, 1 mM ATP, 0.1 mM PLP, and 4 mM lysine). LA1 solutions of different pH levels were generated using acetate, HEPES, or TAPS buffers at a concentration of 50–100 mM. Total cell protein (25 μg/assay) was dissolved in buffer LA2 (25 mM MES, pH 6.0, 0.1 mM PLP, and 4 mM lysine). Assays were conducted in 100-μl volumes at 37 °C using either a quartz plate or Eppendorf tubes. At specific time points, 15-μl aliquots were removed and added to an equal volume of 1 M Na_2CO_3 stop solution. Subsequently, 15 μl of 10 mM 2,4,6-trinitrobenzenesulfonic acid (TNBS) was added, and samples were heated at 40 °C for 5 min to allow the formation of cadaverine-TNBS and lysine-TNBS adducts. Cadaverine-TNBS (*N*,*N*′-bistrinitrophenylcadaverine) was extracted using 500 μl of toluene, and the absorbance at 340 nm was measured. An extinction coefficient of 2.5×10^4 M^{-1} cm^{-1} was used (36) to convert absorbance into moles of cadaverine produced.

Growth in LdcI Indicator Media—*E. coli* K12 MG1655 WT, Δ*ravA*, and Δ*cadB* cells were grown in lysine decarboxylase indicator media DI1 (0.3% yeast extract, 0.1% glucose, 0.5% lysine, and 0.0016% bromocresol purple pH indicator) at 37 °C. Samples were taken at selected time points, cells were pelleted by centrifugation, and the absorbance at 590 nm of the bromocresol purple indicator in the cleared lysates was measured.

Extreme Acid Shock Assays—Extreme acid shock assays were adapted from previously described protocols (37). Briefly, *E. coli* K12 MG1655 WT and Δ*ravA* cells were grown in LB media containing 2% glucose at 37 °C for 18 h. Cells were diluted 1/100 into pH 2.5 acid shock media AS1 (40 mM KCl, 80 mM KH_2PO_4, 33 mM H_3PO_4, 1.7 mM sodium citrate, and 20 mM glucose) with and without 1 mM lysine. Samples were incubated at 37 °C for 2 h and then serially diluted in LB media in a 96-well plate. Diluted cells were then spotted onto an LB agar plate and grown up at 37 °C overnight. Growth on plates was examined to determine cell viability.

Northern Blot Analysis—*E. coli* MG1655 cultures were grown in LB media at 37 °C to an A_{600} of 0.6–0.8. Total RNA was isolated using the single step acid guanidinium thiocyanate-phenol-chloroform extraction method as described (38). Briefly, 1.5-ml samples of culture were centrifuged and resuspended in 500 μl of buffer NB1 (4 M guanidinium thiocyanate, 25 mM sodium citrate, 0.5% sodium lauryl sarcosinate, and 0.1 M β-mercaptoethanol). Samples were then passed four times through a 25-gauge needle to facilitate lysis. 0.05 ml of 2 M sodium acetate (pH 4.0), 0.5 ml phenol, and 0.1 ml chloroform-isoamyl alcohol were then added sequentially to the sample. After each addition, the tube was capped and mixed thoroughly by inversion. Samples were then vortexed briefly, incubated on ice for 15 min, and centrifuged at 10,000 × *g* for 20 min at 4 °C. The upper aqueous phase was transferred to a fresh tube, and an equal volume of isopropanol was added. The solution was mixed thoroughly and incubated at −20 °C for 1 h. RNA precipitate was collected by centrifugation at 10,000 × *g* for 30 min at 4 °C. The isopropanol was carefully decanted, and the pellet was resuspended in 0.15 ml of buffer NB1. After thorough mixing, the sample was precipitated again using isopropanol. After centrifugation, the RNA pellet was washed twice with 75% ethanol, and the pellet was resuspended in 50 μl of diethyl pyrocarbonate water. Samples were stored at −80 °C.

20 μg of total RNA was separated on a 1.2% agarose gel containing 6.7% formaldehyde. RNA was transferred to Hybond N+ Nylon membrane (Amersham Biosciences) and was covalently cross-linked to the membrane by UV irradiation using a Stratalinker UV Crosslinker (Stratagene). Probe generation and Northern blotting were carried out using the AlkPhos Direct Labeling and Detection System (Amersham Biosciences). For RavA, the DNA probe used was complementary to bp 623–1497 of the *ravA* gene, whereas for ViaA, the DNA probe used was complementary to bp 719–1452 of the *viaA* gene.

RT-PCR—RT-PCR analysis was performed using the Qiagen OneStep RT-PCR kit as described in the manufacturer's instructions. 2 μg of *E. coli* K12 MG1655 total RNA was used as a template. Amplification was carried out using primers RAVA_forward2 (5′-tatcacggcgccatggctcaccctcatttattag-3′) and VIAA_reverse and primers RAVA_internal_forward (5′-gcgaattccatatgcaacaaattgatgtattgatgaccg-3′) and VIAA_internal_reverse (5′-cgttcgatcacttttttcacg-3′).

Western Blot Analysis—Typically, cell pellets were lysed by sonication, and lysates were centrifuged to remove cellular debris. Supernatant was transferred to a fresh tube, and protein concentration was determined using the Bio-Rad Protein Assay. 5–40 μg of proteins was separated on a 10% SDS-PAGE gel and transferred to Biotrace polyvinylidene difluoride membrane using a Bio-Rad semidry transfer apparatus

as per the manufacturer's instructions. Membranes were then incubated with rabbit polyclonal anti-RavA or anti-LdcI antibodies generated at the Division of Comparative Medicine, University of Toronto. Membranes were then washed and incubated with protein LA-peroxidase. ECL detection reagent (Amersham Biosciences) was used to visualize RNA bands on a Bioflex chemiluminescence detection film (Clonex).

Subcellular Fractionation of E. coli—200 ml of cells grown at 37 °C until an A_{600} of 2.5 was divided into 2 × 100 ml and centrifuged at 4000 × *g* for 10 min at 4 °C. Cell pellets were washed once with buffer SF1 (10 mM Tris-HCl, pH 7.1, and 30 mM NaCl) and then centrifuged again. One pellet was used for the isolation of perisplasmic and cytoplasmic proteins, and the other pellet was used for the isolation of membrane proteins. Periplasmic and cytoplasmic proteins were isolated using a protocol based on a previously described osmotic shock method (39), whereas total membrane proteins were isolated as previously described (40).

Size Exclusion Chromatography—A calibrated Superose 6 HR 10/30 column connected to an AKTA fast-protein liquid chromatography system (Amersham Biosciences) was used for size exclusion chromatography. Samples were typically run in buffer SE1 (25 mM Tris-HCl, pH 7.5, 300 mM NaCl, 2.5 mM $MgCl_2$, and 1 mM DTT) in the presence or absence of 1 mM ATP. 0.1 mM PLP was added to the buffer when LdcI or LdcC were included in the sample. The column was calibrated using molecular mass standards (Sigma): thyroglobulin (669 kDa), apoferritin (443 kDa), β-amylase (200 kDa), bovine serum albumin (66 kDa), carbonic anhydrase (29 kDa), and cytochrome *c* (12.4 kDa). All experiments were performed at 10 °C, and absorbance was monitored at 280 nm.

Analytical Ultracentrifugation Analysis of RavA—Sedimentation equilibrium experiments on RavA were carried out at the Ultracentrifugation Service Facility in the Department of Biochemistry at the University of Toronto. 20 μM RavA protein in Buffer AU1 (25 mM Tris, pH 7.5, 300 mM NaCl, 1 mM DTT, and 10% glycerol) containing 0.2 mM ATP was spun at 5000 and 8000 rpm, at 4 °C, in an An-60 Ti rotor in a Beckman Optima XL-A analytical ultracentrifuge. Absorbance was recorded at 230 and 280 nm. Data analysis was performed using the Origin MicroCal XL-A/CL-I Data Analysis Software Package Version 4.0.

Mapping of RavA Domains—7.5 μg of purified RavA protein was dissolved in 140 μl of buffer RD1 (10 mM Tris, pH 7.5, 100 mM KCl, 10 mM $MgCl_2$, 2.5 mM DTT, and 5 mM ATP) and digested with 0.075 μg of trypsin (Roche Applied Science, 1418475) at 4 °C. At specific time points aliquots of digested protein were removed and separated using SDS-PAGE. Sample preparation of bands for mass spectrometry was adapted from a previously described method (41). Briefly, the samples were processed in 500 μl of PCR grade tubes. The gel band was cubed and washed sequentially in high-performance liquid chromatography grade water (VWR, EM-WX0004-1) and 100 mM ammonium bicarbonate (Sigma, A6141). The gel cubes were dehydrated between the following steps with 100% acetonitrile (VWR, EM-AX0151-1): gel cubes were reduced with 1 mM DTT (Sigma D9163) at 50 °C for 30 min and alkylated with 55 mM iodoacetamide (Sigma, I1149) at room temperature for 20 min in the dark. Gel cubes were dehydrated with acetonitrile washes and SpeedVac-treated to remove acetonitrile. Protein was digested by swelling the cubes with 50 μl of 0.1 ng/μl trypsin in 50 mM ammonium carbonate and 0.1% calcium chloride overnight. The tryptic peptides were extracted from the gel slices by shaking with two washes of 150 μl of 100 mM ammonium carbonate buffer at 37 °C for 45 min. Liquid from the overnight digestion and two extractions were pooled on ice and acidified with 2 μl of 1% glacial acetic acid (VWR EM-AX0073-6). Peptides were desalted and concentrated using C18 resin (Sigma, H8261) by a batch method. Final volume was 10 μl of extracted tryptic peptides in 65% acetonitrile and 1% acetic acid. A 1-μl aliquot of tryptic peptide sample was mixed with 1 μl of a saturated α-cyano-4-hydroxycinnamic acid (Sigma, C2020) solution in 30% acetonitrile and 1% acetic acid and spotted onto a stainless steel matrix-assisted laser desorption ionization sample plate (Bruker Daltonics). For high mass bands, the samples were concentrated and desalted by a batch method similar to tryptic peptide clean up but with the exception that C4 resin (Sigma) was used. The final volume was 15 μl in 65% acetonitrile and 1% acetic acid. A 1-μl aliquot of partial proteolysis sample was mixed with 1 μl of a saturated sinapinic acid (Sigma, D7927) solution in 30% acetonitrile and 1% acetic acid and spotted onto a stainless steel matrix-assisted laser desorption ionization sample plate.

High mass samples were analyzed in a Bruker Reflex III (Bruker Daltonics) in high mass linear mode with a high mass detector. Carbonic anhydrase (Sigma, C3934) and lysozyme (Sigma, L7651) were used as external calibrants. Tryptic peptides were analyzed in a Bruker Reflex III (Bruker Daltonics) in reflector mode. Samples were internally calibrated using trypsin peptide peaks. Mass mapping was done using PAWS (Genomic Solutions) against the known sequence of the protein. The tryptic peptide fingerprint of a gel band was used to determine an approximate region for the partial proteolysis fragment from the full sequence. The observed high mass was then used to define the exact cut sites for the partial proteolysis fragments.

Electron Microscopy—For preparation of negatively stained protein samples, 3 μl of protein solutions was applied to glow-discharged continuous carbon copper grids and left for 1 min before washing with two drops of 1% (w/v) uranyl acetate. The grids were observed with a Philips CM 12 transmission electron microscope with an LaB6 filament at 80 kV. Images were recorded on Kodak SO-163 films at 35,000× magnification in the case of RavA, LdcI, and ATPγS·RavA·LdcI preparations and at 22,000× for the ADP·RavA·LdcI preparation. Negatives were digitized on a Zeiss SCAI scanner at a pixel size of 7 μm, corresponding, at the specimen level, to 0.2 nm and 0.318 nm at 35,000× and at 22,000×, respectively. Image processing was carried out on a Linux workstation using the EM (42, 43), EMAN (44), BSOFT (45), and PFT2 (46)[5] software packages. Images were binned to 0.4 nm or to 0.636 nm at the specimen level.

Image Analysis—For LdcI, 3631 subframes of 88 × 88 pixels containing single particles were extracted interactively from several micrographs at similar defocus of ~600 nm, and low-pass-filtered at 17 Å resolution to remain within the first zero of the contrast transfer function. This data set was translationally but not rotationally aligned relative to the rotationally averaged total sum of the individual images. The aligned data set was subjected to multivariate statistical analysis/EM, which clearly demonstrated the 5-fold symmetry of the LdcI particle. Characteristic class averages were then used as a set of references for multireference alignment/EM followed by multivariate statistical analysis and classification. The resulting class averages were similar to those obtained by reference free alignment and classification routine in EMAN. Five characteristic views were selected to generate an initial three-dimensional model of the LdcI particle by cross common lines. Refinement of the three-dimensional model was, therefore, undertaken with a D5-symmetry imposed (EMAN and PFT2/BSOFT). After convergence, the symmetry was relaxed and the absence of divergence was

[5] D. M. Belmap, J. F. Conway, and J. B. Heymann (2004) www.niams.nih.gov/rcn/labbranch/lsbr/software/pft2_em3dr2/pft2_em3dr2.htm.

verified. The resolution of the reconstruction was determined via Fourier shell correlation to be ~20 Å according to the 0.5 criterion. The handedness was not determined.

For ADP·RavA·LdcI and ATPγS·RavA·LdcI complexes, the procedure was similar to the one described above for LdcI alone. 2902 subframes of 80 × 80 pixels (6.36 Å/pixel) were extracted from the images of ADP·RavA·LdcI and 2629 subframes of 112 × 112 pixels (4 Å/pixel) from the images of ATPγS·RavA·LdcI. The data were low-pass-filtered at 18 Å, which is again within the first zero of the contrast transfer function. In this case, the majority of particles were present in a side-view orientation or as tilted views. Given the appearance of the side views it was obvious that the RavA·LdcI complex looked like a sandwich of two LdcI molecules bridged together by densities that might be attributed to RavA. Therefore, the reconstruction was performed imposing a 5-fold symmetry of the complex, although, contrary to the situation with LdcI alone and due to the under representation of top views, it could not be revealed by multivariate statistical analysis. Once again, classification allowed selection of five characteristic views used for generation of an initial 5-fold symmetric model by cross common lines. In addition, two alternative three-dimensional models were created by using the same five characteristic views supplemented by a simulated top view. The two simulated top views were composed of the previously determined top view of LdcI alone surrounded by five symmetrically distributed blobs of density positioned either as a radial extension of each LdcI subunit or in the middle between two adjacent subunits to reach the dimensions compatible with the observed side views of the RavA·LdcI complexes. After the refinement in EMAN and PFT2/BSOFT with a D5-symmetry imposed, all the models converged to the same final structure, which remained stable upon symmetry relaxation. The reconstructions of the two complexes ADP·RavA·LdcI and ATPγS·RavA·LdcI looked indistinguishable from each other and had a similar final resolution. The resolution of the reconstructions was estimated to be ~30 Å via Fourier shell correlation but was most probably asymmetric due to the preferential adsorption of the particles on the carbon surface in a side-view orientation. Moreover, if some of the nucleotide·RavA·LdcI complexes were built by LdcI molecules linked not by five but by four or three RavAs, for example, such heterogeneity of the preparation would also lead to a deterioration of the achievable resolution.

RESULTS

RavA Represents a Distinct Subfamily Within the MoxR AAA+ Family—Initially, phylogenetic analysis of the MoxR AAA+ family was carried out to determine the major subfamilies within this family. A phylogenetic tree was generated using 156 MoxR AAA+ sequences, which belong to MoxR Clusters of Orthologous Groups 0714 (COG0714) (National Center for Biotechnology Information, National Institutes of Health) (24). The tree reveals the presence of six distinct subfamilies: MoxR-Proper, CGN, RavA, YehL, APE0892, and PA2707 (Fig. 1*A*). The first five of these groups are consistent with those reported earlier (2). None of the proteins of the RavA, YehL, APE0892, and PA2707 subfamilies have yet been characterized; however, limited work with members of the MoxR-Proper and CGN subfamilies has suggested that the MoxR AAA+ proteins function as molecular chaperones. Closer examination of the 36 genes in the RavA subfamily reveals that 33 of these occur immediately adjacent to genes encoding proteins containing VWA domains (Fig. 1*B*). The co-occurrence of MoxR AAA+-containing genes with those encoding proteins containing VWA domains is a common feature within the MoxR family as a whole (data not shown) but appears with particularly high frequency among the RavA subfamily. This suggests a functional linkage between the RavA AAA+ proteins and their VWA-containing counterparts. In the case of *E. coli* RavA, the VWA-containing protein is YieM, which we have renamed ViaA.

Examination of a ClustalW (27) alignment of all 36 RavA sequences revealed the presence of a number of highly conserved signature sequences in the *E. coli* K12 MG1655 RavA sequence (marked in *red* in Fig. 2). Upon comparison to common AAA+ signature sequences (1), it is observed that many of these conserved residues distinguish RavA proteins from other AAA+ proteins. At the N terminus, the Box II motif contains two highly conserved residues, an Arg and hydrophobic residue (Leu in the RavA sequence). The Walker A motif contains a number of highly conserved residues, but most of these are common to all AAA+ proteins. One feature of note, however, is that members of the RavA subfamily favor an alanine residue in place of the more commonly observed glycine of the classical "GK(S/T)" motif. A series of highly conserved residues also exist in the Box IV and Box IV′ motifs. Based upon comparison to published alignments, at least part of the sequence in this region may lie on a small "insert" in the second helix of the AAA+ core module (2). The Walker B motif also contains a number of highly conserved residues. Most of these are common to all AAA+ proteins, however, the conserved tryptophan/phenylalanine residue is particularly unique to RavA and may have important functional significance to RavA proteins. A unique, highly conserved LP motif also exists immediately prior to the Walker B motif.

Within Box VI, which follows the Walker B, members of the MoxR family possess a highly conserved LL*XX*Φ*X*E motif, with members of the RavA subfamily possessing a slightly extended version L*X*N*X*LL*XX*ΦNE(R/K) motif, where Φ corresponds to Ile, Leu, Val, or Met. The significance of this conserved region is unclear. The Sensor 1 region contains a highly conserved PΦX_5ASN*X*ΦP motif. The conserved Asn residue appears to correspond to the AAA+ Sensor 1 residue (5), responsible for interacting with the gamma phosphate of bound ATP. The conserved Ser is also very common in AAA+ in general. The rest of this conserved sequence, however, appears to be specific to RavA/MoxR proteins.

A conserved L*X*A*X*YDR*XXX*R motif exists in Box VII-Box VII′ region. This region contains the conserved arginine finger of AAA+ proteins, believed to be responsible for mediating intersubunit communication in response to ATP hydrolysis (5). The first Arg residue in the conserved motif may correspond to the arginine finger. Some additional conserved hydrophobic residues also exist in Box VII′ and in the sequence following Box VII″. The Sensor 2 region contains a short stretch of conserved residues, SDRR. One of the arginines is expected to correspond to the conserved Sensor 2 residue present throughout most of the AAA+ superfamily. This residue is believed to be responsible for sensing ATP and mediating movements between the AAA+ core domain and small α-helical domain (5). The Ser residue and first Arg are common to many MoxR proteins in general, however, the Asp and second Arg residues appear to be unique to RavA subfamily members and may be important for a specific function in these proteins. Some additional conserved hydrophobic residues also exist in this region, however, there is little conservation in the RavA sequences after Sensor 2.

RavA Is a Soluble Cytoplasmic ATPase Consisting of Two Domains—To experimentally determine the domains present in RavA structure, we expressed and purified the protein from *E. coli*. The purified protein was then treated with limited amounts of sequencing grade trypsin for varying amounts of time (Fig. 3*A*). The boundaries of the fragments generated were then determined using mass spectrometry (Fig. 3*B*). Based on this analysis, the protein can be divided into two main

A

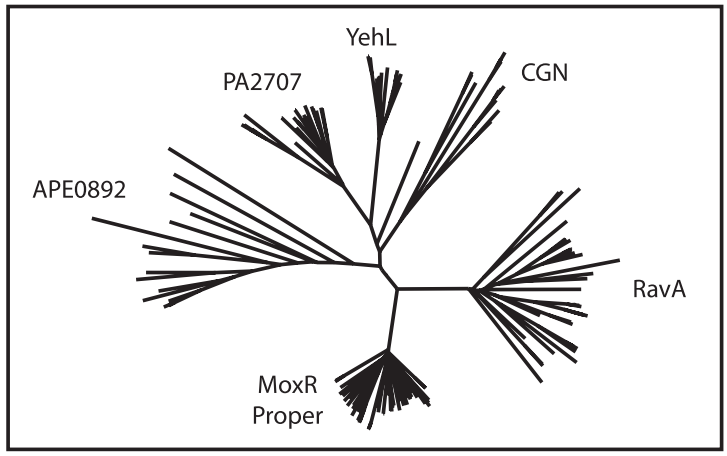

B

#	GI Number	Organism	RavA Subfamily: Adjacent VWA domain-containing protein
1	14601148	*Aeropyrum pernix*	✓
2	66858434	*Anaeromyxobacter dehalogenans 2CP-C*	✓
3	60681677	*Bacteroides fragilis NCTC 9343*	✓
4	29345745	*Bacteroides thetaiotaomicron VPI-5482*	✓
5	57241650	*Campylobacter lari RM2100*	✓
6	34498193	*Chromobacterium violaceum ATCC 12472*	×
7	48853798	*Cytophaga hutchinsonii*	×
8	16131614	*Escherichia coli K12*	✓
9	50118970	*Erwinia carotovora subsp. atroseptica SCRI1043*	✓
10	68140080	*Ferroplasma acidarmanus Fer1*	✓
11	47092621	*Listeria monocytogenes str. 4b H7858*	×
12	2496128	*Methanocaldococcus jannaschii DSM*	✓
13	2495785	*Methanocaldococcus jannaschii DSM*	✓
14	20091041	*Methanosarcina acetivorans C2A*	✓
15	20089152	*Methanosarcina acetivorans C2A*	✓
16	68134507	*Methanosarcina barkeri str. fusaro*	✓
17	68132708	*Methanosarcina barkeri str. fusaro*	✓
18	21228941	*Methanosarcina mazei Go1*	✓
19	21227633	*Methanosarcina mazei Go1*	✓
20	26553847	*Mycoplasma penetrans HF-2*	✓
21	54027784	*Nocardia farcinica IFM 10152*	✓
22	54302311	*Photobacterium profundum SS9*	✓
23	37524086	*Photorhabus luminescens*	✓
24	48478302	*Picrophilus torridus DSM 9790*	✓
25	18313673	*Pyrobaculum aerophilum str. IM2*	✓
26	47571823	*Rubrivivax gelatinosus PM1*	✓
27	16767163	*Salmonella typhimurium*	✓
28	24115049	*Shigella flexneri 2a str. 301*	✓
29	21225846	*Streptomyces coelicolor A3*	✓
30	70606761	*Sulfolobus acidocaldarius DSM 639*	✓
31	15899119	*Sulfolobus solfataricus P2*	✓
32	15920718	*Sulfolobus tokodaii str. 7*	✓
33	15601518	*Vibrio cholera*	✓
34	59713681	*Vibrio fischeri ES114*	✓
35	28900864	*Vibrio parahaemolyticus RIMD 2210633*	✓
36	16120358	*Yersinia pestis*	✓

FIGURE 1. **Phylogenetic analysis of MoxR AAA+ proteins.** *A*, phylogenetic tree generated from 156 MoxR AAA+ proteins belonging to COG0714 as described under "Materials and Methods." Six major subfamilies were identified, including RavA, MoxR Proper, YehL, CGN, APE0892, and PA2707. *B*, 36 members of the RavA subfamily from 32 organisms are listed. The presence or absence of an adjacent VWA domain-containing protein is indicated.

domains: a highly conserved N-terminal domain (Met^{1}–Arg^{347}), which corresponds to the AAA+ module, and a poorly conserved C-terminal domain (Arg^{348}–Cys^{498}) that is predicted to be predominantly α-helical. As is typical for AAA+ modules (1), the N-terminal domain can be separated into two smaller fragments (Fig. 3, *A* and *B*), which appear to correspond to the AAA+ $\alpha\beta$ subdomain (Met^{1}–Arg^{187}) and an α-helical subdomain (Ser^{188}–Arg^{347}). The C-terminal domain of RavA has no known motifs or signature sequences and appears to represent a novel domain of unknown function. The sequence of this domain bears little homology to any other protein sequence in NCBI (48) and is poorly conserved in RavA proteins outside of the enterobacteria subdivision. It is interesting to note that the *E. coli* RavA sequence after residue Ala^{288} is highly enriched in glutamines (Fig. 2).

Subsequently, the subcellular localization of RavA was determined. Wild-type and Δ*ravA* cells grown at 37 °C to early stationary phase were lysed and separated into cytoplasmic, periplasmic, and crude membrane fractions. Western blot analysis of these fractions using αRavA antibodies (Fig. 3*C*) clearly showed that RavA is predominantly cytoplasmic. This is consistent with the lack of any predicted signal sequences or transmembrane regions in RavA. A faint band observed in the membrane fractions appears to be nonspecific, as it appears in both the WT and Δ*ravA* strains.

As shown in Fig. 3*D*, purified RavA at 0.4 μM has the highest ATPase activity at neutral to alkaline pH, with the highest activity around pH 7.5. Below pH 7.5, the activity appears to drop rapidly and is minimal below pH 6.0. Complete Michaelis-Menten kinetic analysis was performed at

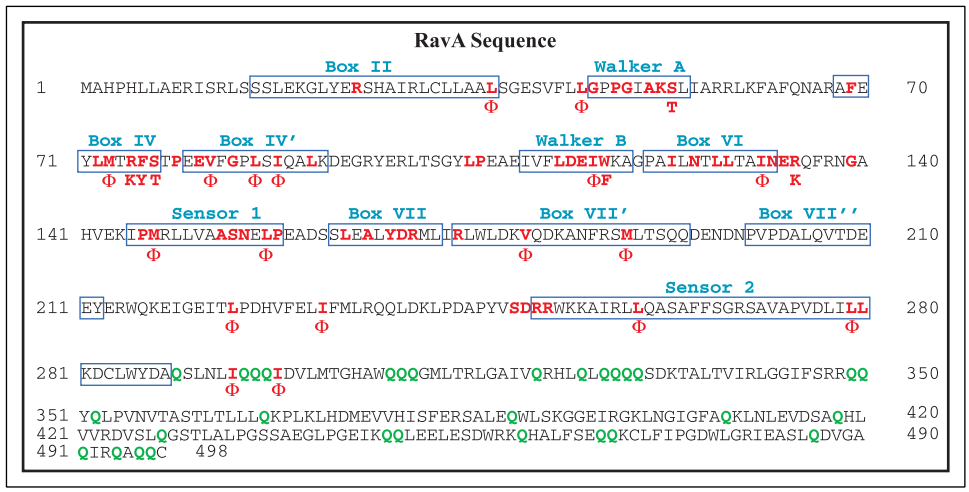

FIGURE 2. **Assignment of highly conserved residues in RavA AAA+ proteins.** The amino acid sequence of RavA from *E. coli* K12 is shown. Major features of the AAA+ module were obtained from published alignments and are shown *boxed* (1, 2). Sites of residues conserved in >90% of 36 ClustalW-aligned RavA subfamily members are *colored red*. Conservation is based on the following amino acid groupings: ILVM, KR, DE, ST, YFW, and NQ. Ala, Cys, Pro, His, and Gly are not grouped. In almost all cases a specific residue highlighted in the RavA sequence is one of the most frequently occurring throughout the RavA subfamily. Variant conserved residues present in at least 20% of subfamily members are indicated in *single-letter code* below the RavA sequence. In the case of the ILVM group, a "Φ" symbol below a residue is used to indicate that at least 20% of subfamily members contain one of these residues. All glutamine residues after the Sensor II motif are shown in *green*.

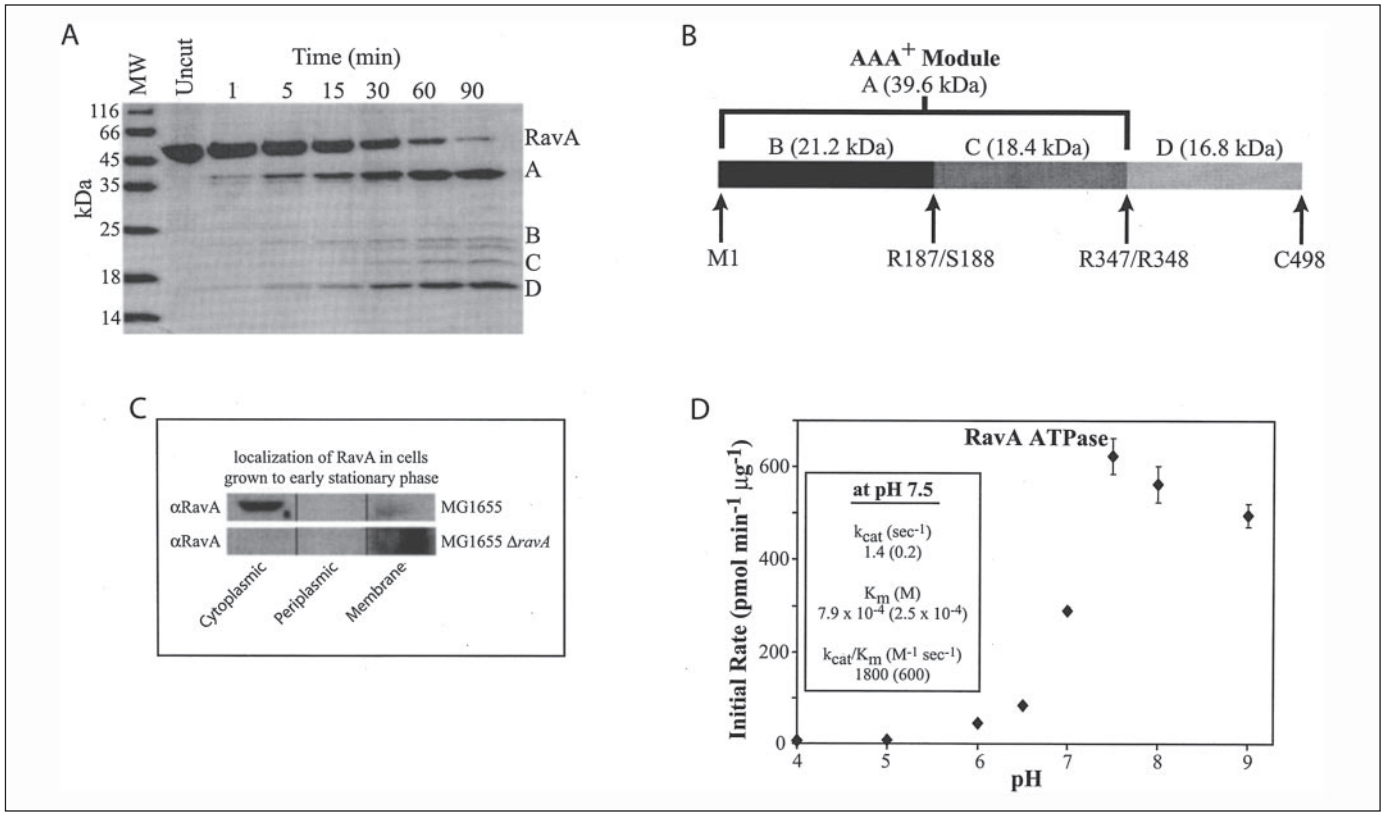

FIGURE 3. **Domain mapping, localization, and ATPase activity of RavA.** *A*, SDS-PAGE analysis of RavA tryptic digest at different time points are shown. Major bands are labeled. *B*, schematic diagram of the trypsin cleavage sites and proposed tryptic domains of RavA, as identified by mass spectrometry is shown. The four discrete fragments, labeled *A*–*D*, refer to the bands indicated in *A*. *C*, localization of RavA in WT and Δ*ravA E. coli* cells grown to stationary phase in LB media. Cytoplasmic, periplasmic, and membrane fractions are shown. RavA protein is localized to the cytoplasm. A faint band present in the membrane fraction is nonspecific as it is present in both WT and Δ*ravA* strains. *D*, ATPase activity of purified RavA protein at various pH value. k_{cat}, K_m, and k_{cat}/K_m values are given for pH 7.5 (*inset*).

pH 7.5 (Fig. 3*D*, *inset*). The k_{cat} and K_m values for RavA ATPase are in a similar range to those obtained for other AAA+ proteins such as HslU (49), NtrC (50), and Lon (51). Furthermore, RavA also has GTPase activity. GTP hydrolysis appears to be much slower than ATP hydrolysis at lower enzyme/substrate concentrations but reaches comparable levels with increasing amounts of enzyme/substrate (data not shown). This effect may be the result of a lower ability of GTP *versus* ATP to promote RavA oligomerization (data not shown).

ravA and viaA Genes Form an Operon under the Direct Control of σ^S—The *ravA* and *viaA* gene sequences encode predicted proteins of similar length consisting of 498 and 483 amino acid residues, respectively. The genes reside on the *E. coli* chromosome close to the origin of replication (OriC) (52), ~2200 bp clockwise from OriC, and the genes are transcribed in the counterclockwise direction. Interestingly, the 5′-end of the ViaA coding region overlaps the 3′-end of the RavA coding sequence by seven bases (Fig. 4*A*). Such an overlap might hint to the presence of an ancient gene whose sequence was a fusion of the *ravA* and *viaA* gene sequences.

To determine whether *ravA* and *viaA* are on the same operon, Northern blot analysis was carried out on *E. coli* MG1655 wild-type (WT), MG1655 Δ*ravA*, and MG1655 Δ*viaA* cells. The Δ*ravA* cells have most of the RavA ORF deleted: from 13 bp upstream of the 'atg' start codon to bp 1431 (Fig.

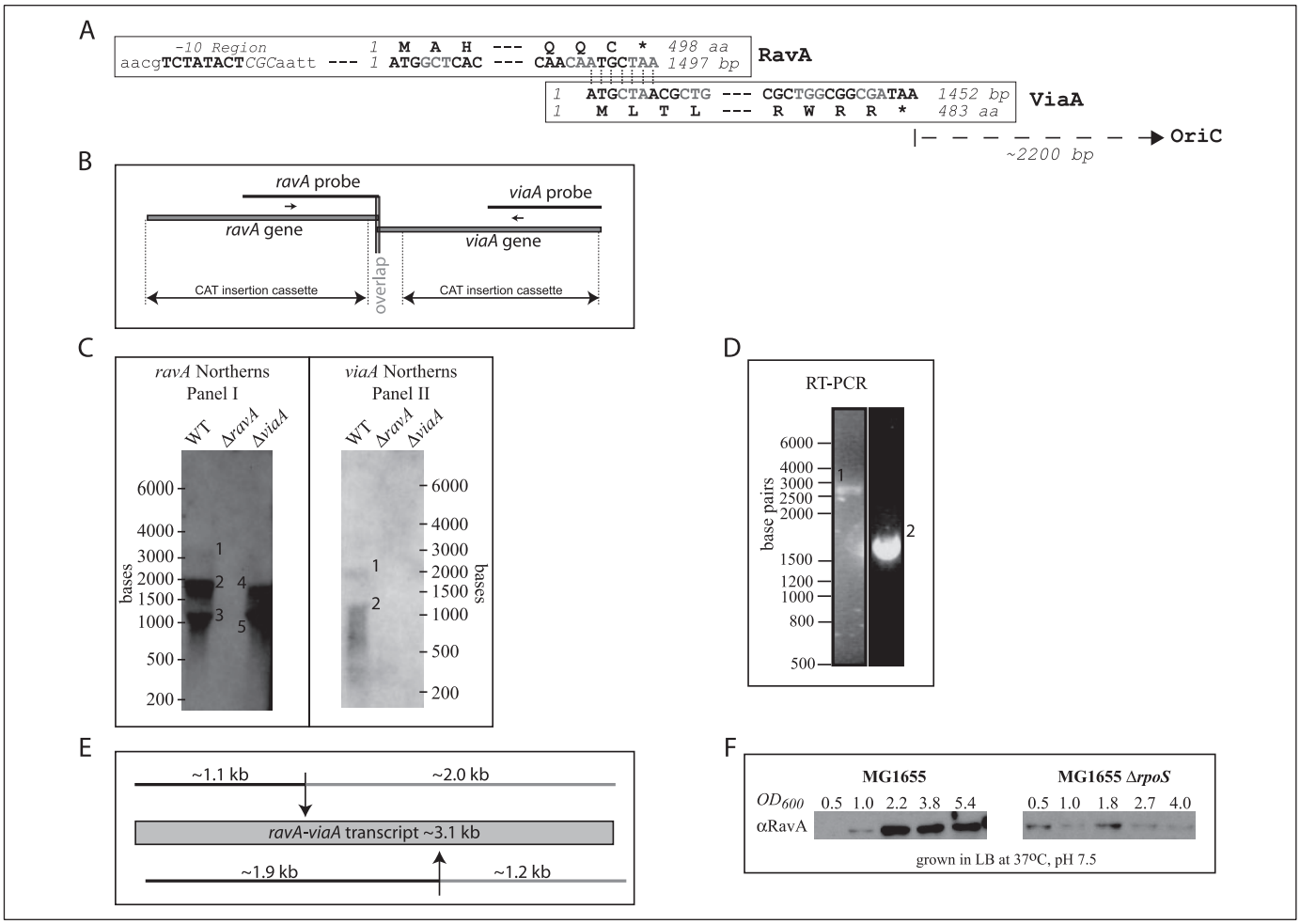

FIGURE 4. ***ravA-viaA* gene organization in *E. coli*.** *A*, the overlap between the RavA and ViaA ORFs is shown. The σ^S consensus sequence in the predicted RavA −10 promoter region is indicated in *uppercase*, with *bolded* residues exactly matching the consensus sequence (53). *B*, scaled schematic showing the areas of the *ravA* and *viaA* genes, which hybridize to the probes used in the Northern blots, and the regions replaced by the chloramphenicol acetyl transferase (*CAT*) resistance cassettes in the deletion strains. Sites of internal primers used in RT-PCR, indicated by *small arrows*, are also shown. *C*, Northern analysis of *ravA* and *viaA* in WT, Δ*ravA*, and Δ*viaA* strains. Observed bands are numbered (see text). *D*, RT-PCR confirmation of *ravA-viaA*-containing transcript. *Band 1* was amplified using RavA and ViaA terminal primers. *Band 2* was amplified using RavA and ViaA internal primers. *E*, scaled schematic showing estimated cleavage sites within the ~3.1-kb *ravA-viaA*-containing transcript and predicted product sizes. *F*, Western blot analysis of RavA protein levels in WT and Δ*rpoS* cells grown in LB at 37 °C. RavA protein expression is significantly induced toward late log/early stationary phase in WT cells. This induction is not observed in the Δ*rpoS* cells, consistent with *ravA* being regulated by σ^S.

4*B*). This deletion does not disrupt the ViaA ORF. The Δ*viaA* cells contain a deletion of bp 166–1437 of the ViaA ORF. The cells were grown in LB media at 37 °C to mid-log phase; subsequently, total RNA was isolated and probed with alkaline phosphatase-labeled DNA probe complementary to bp 623–1497 of the *ravA* gene or complementary to bp 719–1452 of the *viaA* gene (Fig. 4, *A* and *B*). Wild-type cells clearly show the presence of two different *ravA* mRNA transcripts of ~1900 and 1100 bases in size (Fig. 4*C*, *bands 2* and *3*, respectively, in the *first lane* of *panel I*). Low levels of an even larger transcript of ~3100 bases are also detected (Fig. 4*C*, *band 1* in the *first lane* of *panel I*). RT-PCR analysis using forward and reverse primers complementary to the 5′-end of the *ravA* ORF and the 3′-end of the *viaA* ORF, respectively, confirms the existence of the larger transcript (Fig. 4*D*, *band 1*). In addition, RT-PCR using a forward primer internal to the *ravA* ORF and a reverse primer internal to the *viaA* ORF also produces a product (Fig. 4*D*, *band 2*), further supporting the existence of these two genes on a single transcript. *viaA* transcript is detected as distinct bands of ~2000 and 1200 bases (Fig. 4*C*, *bands 1* and *2*, respectively, in *first lane* of *panel II*). A larger transcript is not detected in the *viaA* blot, likely a reflection of lower probe sensitivity.

These data suggest that *ravA* and *viaA* exist as a single operon, consistent with the lack of a predicted *viaA* promoter sequence. The full-length ~3100 bases transcript appears to be inherently unstable, however, and undergoes at least two distinct internal cleavage events shown schematically in Fig. 4*E*. The first of these cleavages produces the ~1900-base fragment observed in the *ravA* blot (Fig. 4*C*, *band 2* in the *first lane* of *panel I*) and the ~1200-base fragment observed in the *viaA* blot (Fig. 4*C*, *band 2* in the *first lane* of *panel II*). The second cleavage produces the ~1100-base fragment observed in the *ravA* blot (Fig. 4*C*, *band 3* in the *first lane* of *panel I*) and the ~2000-base fragment observed in the *viaA* blot (Fig. 4*C*, *band 1* in the *first lane* of *panel II*). Whether or not these cleavage events have a regulatory role is currently under investigation.

Northern blot analysis of MG1655 Δ*ravA* show that the deletion of the *ravA* gene results in the loss of all mRNA species (Fig. 4*C*, *lane 2* in *both panels*). On the other hand, Northern blot analysis of MG1655 Δ*viaA* using the probe for *ravA* shows the presence of an ~1700-base transcript and the previously observed ~1100-base transcript (Fig. 4*C*, *bands 4* and *5*, respectively, in *lane 3* of *panel I*). The ~1700-base transcript is slightly smaller than the ~1900-base fragment observed in wild-type cells (Fig. 4*C*, *band 2* in *lane 1* of *panel I*) probably resulting from earlier termination of transcription due to the presence of the deletion cassette (Fig. 4*B*). These results confirm that the *ravA* and *viaA* genes form a single operon.

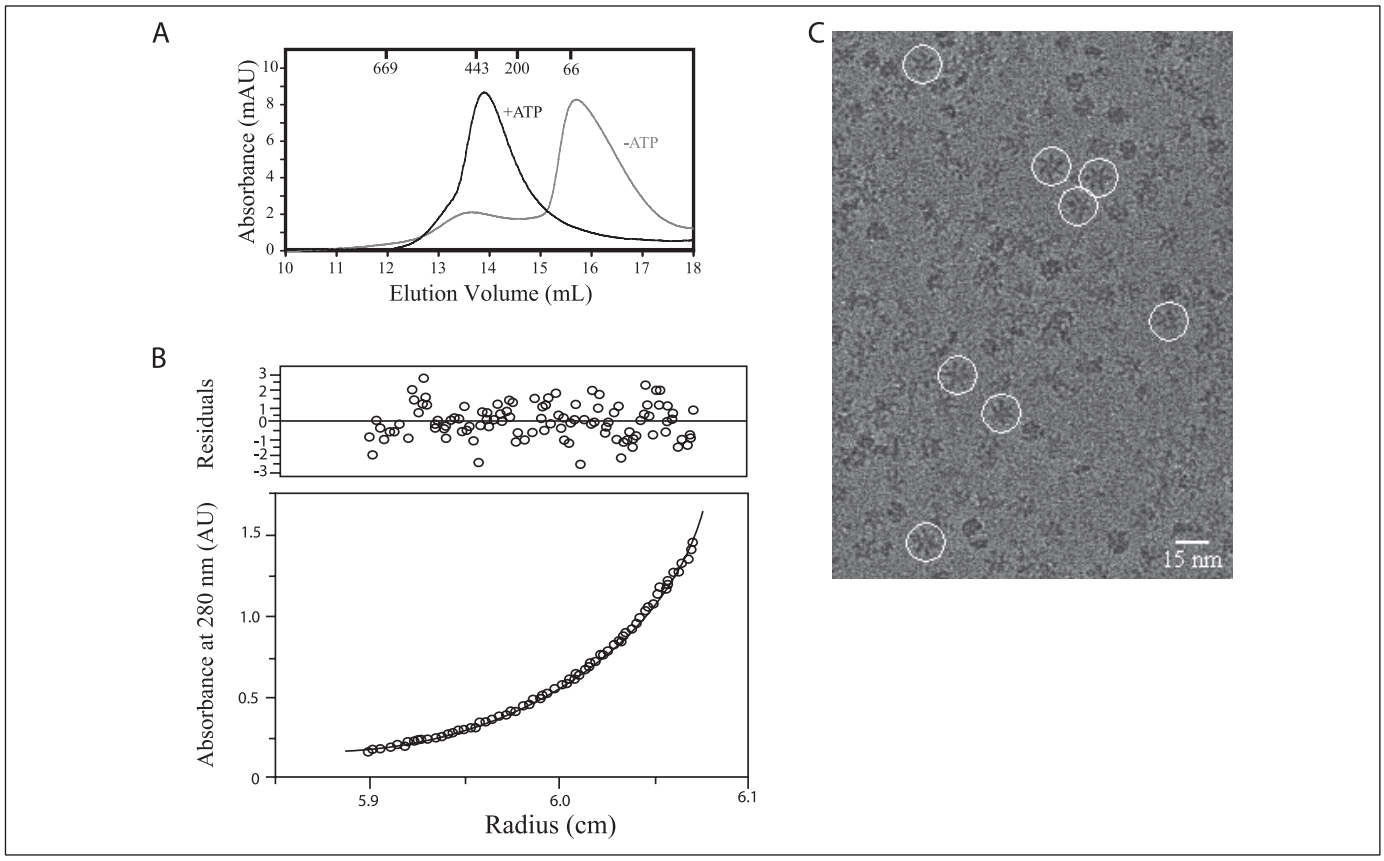

FIGURE 5. **Analysis of RavA oligomerization.** *A*, size exclusion chromatography analysis, using a Superose 6 HR 10/30 column, of 3 μM RavA in the presence and absence of 1 mM ATP. In the absence of ATP, RavA migrates mainly as a small, apparently monomeric species. In the presence of ATP, RavA forms a larger species near the 443-kDa marker. Similar results were obtained when using ADP. *B*, sedimentation equilibrium analysis of 20 μM RavA in the presence of 0.2 mM ATP. RavA exists as a monodisperse species with an average molecular mass of 310 kDa, roughly the size expected of a hexameric oligomer. *C*, analysis of RavA by electron microscopy. Shown are negatively stained RavA particles in the presence of ADP. Some particles that could be attributed to hexamers are *circled*.

Analysis of the sequence immediately upstream of the *ravA* gene reveals the presence of a highly conserved σ^S promoter consensus sequence (Fig. 4*A*) (53). This consensus sequence has been shown to be present in genes that are up-regulated in stationary phase. Consistent with this, Western blot analysis of MG1655 cells shows a significant induction of RavA levels as cells approach late log/early stationary phase (Fig. 4*F*, *left panel*). Such an induction does not occur in an MG1655 Δ*rpoS* strain, although constant levels of RavA protein appear to be present at all times (Fig. 4*F*, *right panel*). The data suggest that RavA induction is partially dependent on the stationary phase sigma factor σ^S, likely in a direct manner. The presence of low, constitutive levels of RavA protein in the Δ*rpoS* strain suggests that the *ravA* promoter may display conditional selectivity allowing its expression to be regulated by other sigma factor(s) (*e.g.* σ^{70}). Such conditional promoter selectivity has been reported for other *E. coli* genes, for instance *dps* and *yaiA*, whose expression may be regulated by either σ^S or σ^{70}, depending on cellular conditions (53).

RavA Forms a Hexameric Oligomer—Many AAA+ proteins typically function as oligomeric rings (6); therefore, the nature of the oligomeric state of RavA was investigated using size exclusion chromatography and analytical ultracentrifugation. Size exclusion chromatography analysis using 3 μM RavA revealed that the protein forms oligomeric species and that this oligomerization is enhanced in the presence of nucleotide (Fig. 5*A*). The largest species formed runs near the 443-kDa marker. To more accurately confirm the size of this species, analytical ultracentrifugation sedimentation equilibrium studies were performed in the presence of ATP. The best fit to the data set corresponds to a monodisperse species of ~310 kDa in size (Fig. 5*B*). This molecular weight corresponds closely with that expected of a hexameric species. Thus we propose that the functional state of RavA is a hexameric oligomer in the presence of nucleotides. Sedimentation equilibrium experiments in the absence of nucleotides revealed the existence of a range of smaller species (data not shown), consistent with our size exclusion results.

Negative stain electron microscopy of RavA in the presence of ADP, ATP, or non-hydrolyzable ATP analogues invariably showed a mixture of different oligomeric states of the protein, ranging from monomers to bigger oligomers. The top-view appearance of the largest oligomers clearly favored their hexameric composition (Fig. 5*C*). However, due to the inhomogeneity of RavA oligomeric states on the grid and the resulting difficulty in unambiguous identification of corresponding side views, no attempts have been made to obtain a three-dimensional reconstruction of the RavA hexamer (however, see below).

RavA Binds to the Inducible Lysine Decarboxylase LdcI/CadA—In an effort to determine the function of RavA, experiments were carried out in an attempt to identify its interacting partners. *E. coli* DY330 strain (30, 31), in which a TAP tag (54) was fused C-terminally to the endogenous *ravA* chromosomal gene, was used for pull-down experiments (33). When RavA-TAP was isolated from cells grown to stationary phase in TB-rich media at 37 °C, the inducible cytoplasmic lysine decarboxylase (LdcI) was found to be strongly bound to RavA (Fig. 6*A*). LdcI (also termed CadA, SwissProt name DCLY_ECOLI, SwissProt number P0A9H3) is a pyridoxal phosphate (PLP, a vitamin B6 derivative)-dependent decameric enzyme (55, 56), which plays a major role in the acid stress response in bacteria (57–59). LdcI decarboxylates a lysine to pro-

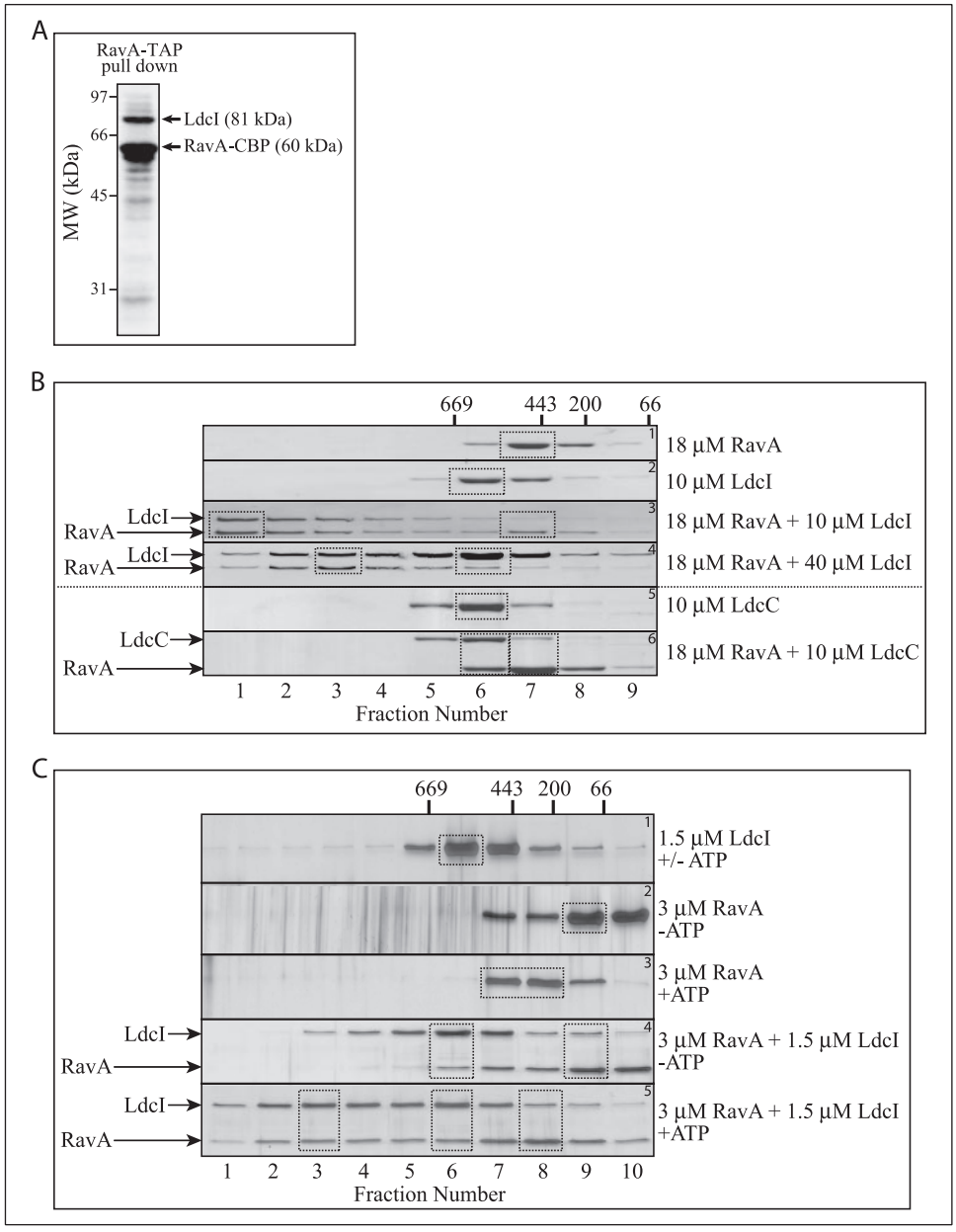

FIGURE 6. **RavA interacts with the inducible lysine decarboxylase (LdcI/CadA).** *A*, pull-down of endogenous, C-terminally TAP-tagged RavA. Identification of the bands by mass spectrometry reveals that RavA interacts with the inducible lysine decarboxylase enzyme, LdcI (*upper band*). The *middle band* corresponds to RavA-CBP (calmodulin binding peptide, which remains after tobacco etch virus cleavage). The band below RavA is a truncation product. *B*, analysis of the interaction of purified RavA, LdcI, and LdcC using size exclusion chromatography in the presence of 1 mM ATP. *Boxes* indicate major peaks. *C*, interaction of RavA and LdcI, at lower concentrations, in the presence and absence of 1 mM ATP.

duce the polyamine cadaverine, which is then pumped out of the cell by an inner membrane lysine/cadaverine antiporter protein, CadB (59, 60). This process removes a proton from the cell cytoplasm and reduces the acidification of the intracellular environment. The genes *cadB* and *ldcI*/*cadA* are on the same operon (60, 61), and the operon is activated by an inner membrane anchored transcription activator, CadC, that binds a P*cad* element in the promoter region of *cadBA* (61). The regulation of *cadBA* transcription is rather complex. The operon is induced by low external pH, by the presence of exogenous lysine, and under anaerobic conditions (55, 62). The binding of RavA to LdcI leads us to speculate that RavA might also be involved in the bacterial stress response or that the interaction between the two proteins is regulatory in nature.

Analysis of the binding of RavA to LdcI was carried out using size exclusion chromatography (Fig. 6, *B* and *C*). All experiments shown in Fig. 6*B* were performed in the presence of 1 mM ATP. 18 μM RavA protein migrates as a single species with an apparent molecular mass of ~440 kDa representing the hexameric species (Fig. 6*B*, *panel 1*, *top panel*). 10 μM LdcI (Fig. 6*B*, *panel 2*) also elutes as a single species, with an apparent molecular mass of 600 kDa probably representing the decameric species that is known to be formed by LdcI (also see below) (55, 56). A mixture of 10 μM LdcI with excess RavA (18 μM) results in a large shift in the migration of both species indicating a strong interaction (Fig. 6*B*, *panel 3*). A range of higher order oligomers are formed, with the predominant complex (*boxed*) migrating at or near the void volume of the column, suggesting a size of ~50 MDa or greater. The predominant complex formed changes if 18 μM RavA is incubated with ~2-fold excess of LdcI (40 μM). The formed complex elutes within the column volume, and its molecular mass is 3–5 MDa as estimated by sedimentation equilibrium experiments (Fig. 6*B*, *left box* in *panel 4* and data not shown). We term this complex the fraction three complex (FTC), which, as discussed below, might be the physiologically relevant RavA·LdcI complex.

E. coli contains another protein that is a very close paralogue of LdcI. This protein is the constitutive lysine decarboxylase LdcC (SwissProt name DCLZ_ECOLI, SwissProt number P52095). LdcI and LdcC are 69% identical and 84% similar as determined using pairwise BLAST P

analysis. LdcC is expressed in *E. coli* at very low levels, and its exact role in the cell remains unclear (63, 64). Like LdcI, LdcC is also a PLP-dependent enzyme that decarboxylates lysine and possibly assembles into a decamer (63, 64) (Fig. 6*B*, *panel 5*). However, the enzymatic activity profile and stability of LdcC differ from that of LdcI (63, 64). Due to the high sequence similarity between LdcC and LdcI, we expected that LdcC might also bind RavA, however, we were surprised to find that there is no significant interaction between RavA and LdcC (Fig. 6*B*, *panel 6*). The specific interaction of RavA with LdcI and not LdcC possibly indicates that RavA is a stress response protein.

The size of the LdcI oligomer (decamer) is unaffected by the presence or absence of ATP (Fig. 6*C*, *panel 1*, *upper panel*) or by LdcI concentration (compare elution profile of 10 μM LdcI in Fig. 6*B*, *panel 2*, to the elution profile of 1.5 μM LdcI in Fig. 6*C*, *panel 1*). As shown in Fig. 6*C*, the size of the RavA·LdcI complex is dependent upon RavA oligomerization. 3 μM RavA in the absence of ATP predominantly elutes at ~60 kDa representing a monomeric species, whereas, in the presence of ATP, 3 μM RavA elutes as the larger hexameric species (Figs. 5*A* and 6*C*, *panels 2* and *3*). LdcI binds to 3 μM RavA in the absence and presence of ATP (Fig. 6*C*, *panels 4* and *5*), however, the size of the complex is smaller in the absence of ATP as compared with when ATP is present. These data indicate that LdcI probably does not promote the oligomerization of RavA in the absence of nucleotide. In Fig. 6*C* (*panel 5*), the FTC is also observed.

Similar interactions were observed between RavA and LdcI when ADP was added to the buffer rather than ATP. Furthermore, the inclusion of lysine or cadaverine or the removal of the LdcI cofactor PLP from the buffer did not affect the interaction between RavA and LdcI (data not shown). These observations clearly indicate that the interaction between RavA and LdcI is highly robust and functionally significant.

RavA·LdcI Forms a Very Large Distinctive Cage-like Complex as Visualized by Negative Stain Electron Microscopy—A 20 Å resolution structure of the D5-symmetric LdcI oligomer (Fig. 7, *A–C*) was obtained as described under "Materials and Methods." The existence of a 5-fold symmetry axis in the particle was corroborated by multivariate statistical analysis. Fig. 7*B* shows the pronounced 5-fold symmetrical shape of the top-view class average and the 2-fold symmetry of the side-view class average. Some dimeric dissociation products could always be detected in the background of the micrographs (Fig. 7*A*), in agreement with the early publication of Sabo *et al.* (55). The random orientation of single particles on the carbon film made this specimen particularly suitable for a three-dimensional reconstruction by angular reconstitution approach (Fig. 7*C*). The decamer of LdcI revealed itself as two pentameric rings, tightly stacked together back-to-back and turned ~35° with respect to each other. Each monomer has a globular shape. The relative rotation of the two rings confers a pronounced handedness to the molecule responsible for the "plait-like" appearance of the side view.

Grids prepared by mixing ADP·RavA or ATPγS·RavA and LdcI in equimolar amounts (1.8 μM RavA to 1.8 μM LdcI) looked indistinguishable from preparations of LdcI alone except for a higher protein background attributed to RavA. Remarkably, however, at ~2-fold excess of RavA (3.24 μM RavA and 1.8 μM LdcI in the presence of 3 mM ADP or ATPγS), the background became clean, individual LdcI views virtually disappeared, and most of the protein was present as an amazingly large and apparently homogeneous RavA·LdcI complex. Analysis of the data revealed that the ADP·RavA·LdcI complex contained not only one, but two LdcI decamers sandwiched together and glued by additional densities that certainly arise from RavA (Fig. 7*D*). In this case, however, the particles had a strongly preferred orientation on the grid, and although different class averages could be easily identified as side views and various tilted views, none could be attributed to a true 5-fold symmetrical top view. Nevertheless, even without a top view class average, an initial model could still be constructed from several characteristic tilted views (Fig. 7*E*) by cross common lines technique, provided a 5-fold symmetry is imposed. A refinement with such a model resulted in the reconstruction shown in Fig. 7*F*. The validity of this approach was confirmed by creating two of the possible top views of the complex, composed of the experimentally observed top view of the LdcI alone that was artificially surrounded by five blobs of density. This density was arbitrarily positioned either in the middle between two adjacent LdcI subunits or as a radial extension of each LdcI subunit (see the *first two panels* in Fig. 7*E*). The only restrictions were the 5-fold symmetry of the top view and the experimental dimensions of the ADP·RavA·LdcI complex side view. These two additional sets of views gave rise to two different initial three-dimensional models of the complex, which converged during the refinement process to the same final reconstruction (Fig. 7*F*), identical to the one obtained without any artificial top view.

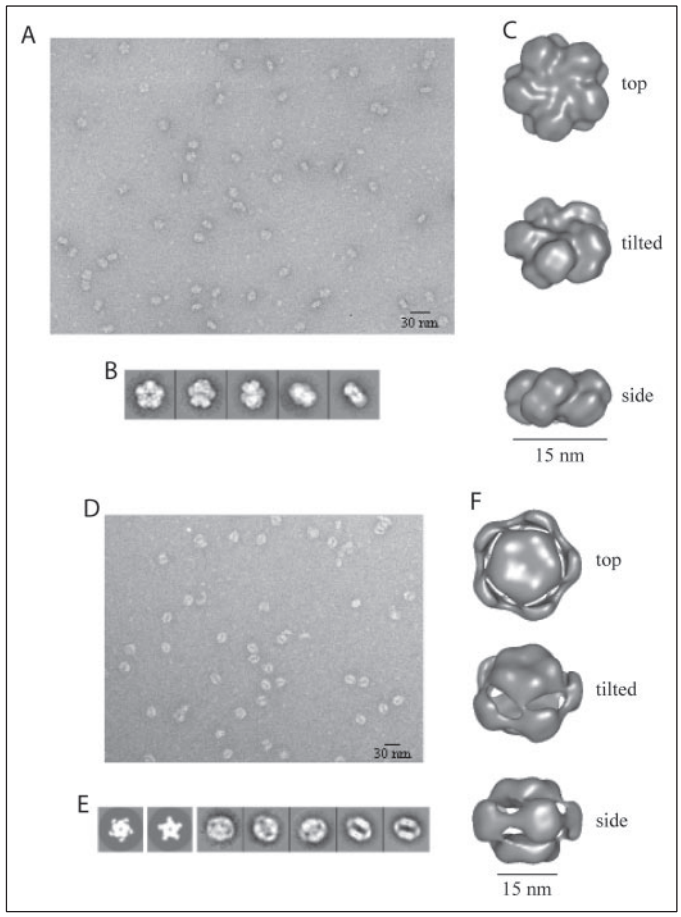

FIGURE 7. **EM analysis of LdcI and RavA·LdcI complex.** *A*, negatively stained LdcI particles. *B*, five characteristic views of LdcI used to calculate an initial three-dimensional model of the particle. *C*, isosurface representations of the three-dimensional reconstruction of LdcI. *D*, negatively stained RavA·ADP·LdcI particles. *E*, two hypothetical 5-fold symmetrical top views of RavA·ADP·LdcI created as described in the text and five characteristic views of RavA·ADP·LdcI used to calculate an initial three-dimensional model of the particle. *F*, isosurface representations of the three-dimensional reconstruction of RavA·ADP·LdcI.

Hence, the RavA·LdcI complex is a unique complex in which five RavA oligomers (at most) bridge two LdcI decamers resulting in a distinctive cage-like structure. Although the volume of the densities attributed to RavA would be consistent with its inclusion in the complex as a hexameric species, the current quality of the reconstruction does not allow us to claim this with absolute certainty. Remarkably, no differ-

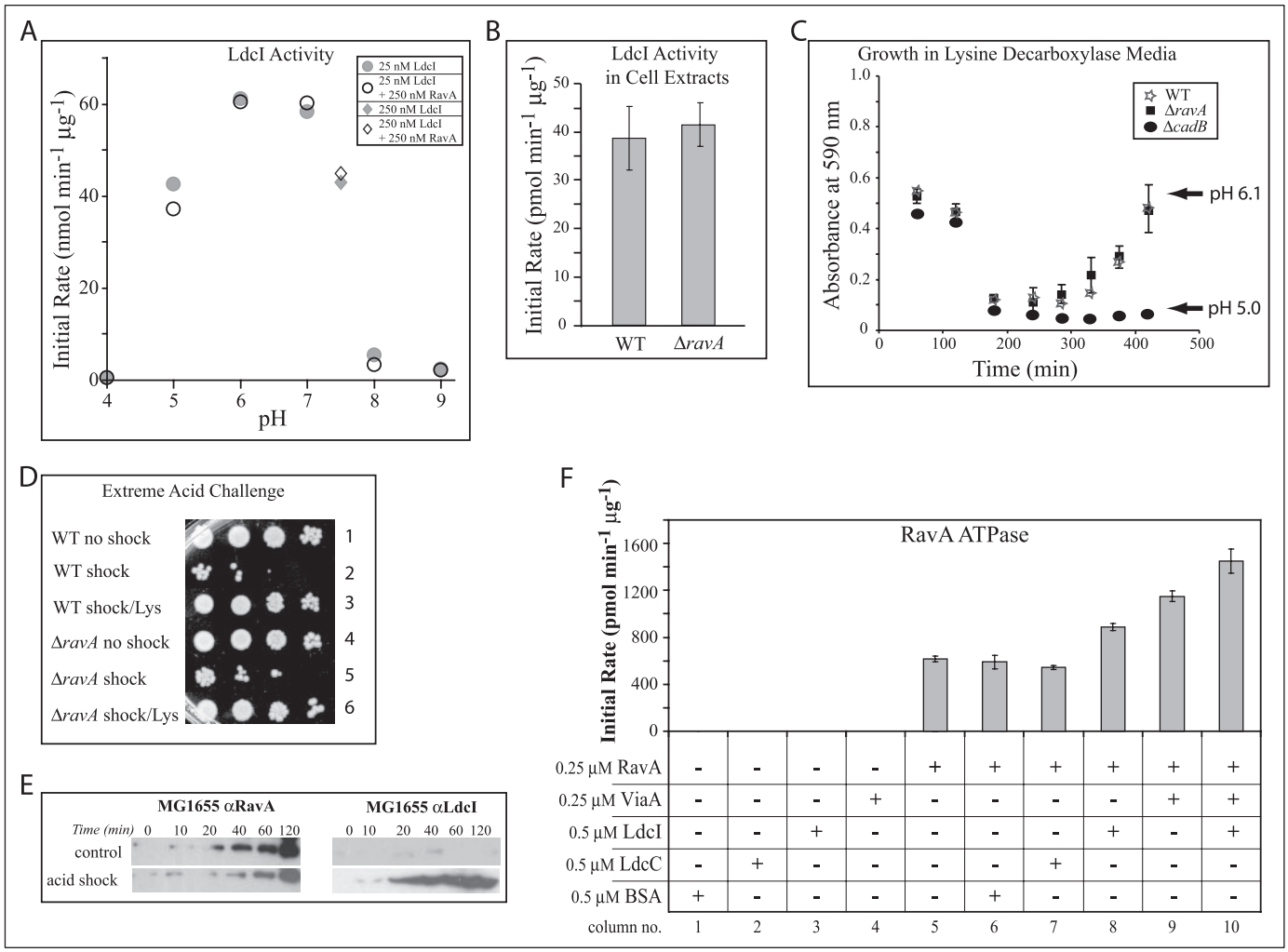

FIGURE 8. **The effect of RavA binding to LdcI on LdcI and RavA activities.** *A*, enzymatic activity of purified LdcI at various pH values in the presence (*empty circles/diamond*) and absence (*filled circles/diamond*) of RavA. *B*, measurement of LdcI activity in soluble cell extracts prepared from WT and Δ*ravA* cells grown in LB in the presence of glucose. Activity is given per microgram of total soluble protein. No difference in activity is observed between strains. *C*, growth of WT, Δ*ravA*, and Δ*cadB* cells in lysine decarboxylase indicator medium containing lysine, glucose as a carbon source, and bromocresol purple as a pH indicator. At various time points, samples were taken and cleared of cells by centrifugation. The pH of the supernatant was recorded by monitoring the change in absorbance at 590 nm of the bromocresol purple indicator. Growth in the presence of glucose results in a decrease in the pH of the medium from pH 6.1 initially to pH 5.0. *D*, extreme acid shock survival assay. The susceptibility of WT and Δ*ravA* strains to extreme acid shock (pH 2.5 for 2 h) was assessed in the presence and absence of lysine to monitor the effectiveness of the CadBA acid stress response system. Both strains suffer a significant decrease in survival in the absence of lysine (compare *rows 2* to *1* and *rows 5* to *4*) but are unaffected by the shock if lysine is present (compare *rows 3* to *1* and *rows 6* to *4*). The CadBA system appears to be equally effective in both strains. 10-fold serial dilutions of cells are shown from left to right. *E*, expression of RavA and LdcI in response to low pH. WT cells were grown in LB media at pH 7.0 to mid-log phase and then shifted to pH 5.0 by addition of low pH media, or kept at pH 7.0 as a control by adding pH 7.0 media. Samples were withdrawn at various time points after addition and the levels of RavA and LdcI were monitored by Western blotting. *F*, effect of BSA, LdcI, LdcC, and ViaA on ATPase activity of purified RavA at pH 7.5, 37 °C.

ences could be observed between the RavA·LdcI complex in ADP and the one in ATPγS (data not shown), at least at the current resolution estimated to be ~30 Å. We believe that the complex seen in Fig. 7 corresponds to the FTC in Fig. 6.

Binding of RavA to LdcI Affects RavA Activity but Not LdcI Activity—The formation of a tight complex between RavA and LdcI either indicates that RavA affects LdcI function or *vice versa*. Because RavA is an AAA+ protein, we expected that it would remodel LdcI in a nucleotide-dependent manner and, hence, affect the activity of the enzyme. LdcI activity was measured at a range of different pH values in the presence and absence of RavA protein (Fig. 8*A*). LdcI activity is greater at neutral pH than at alkaline pH, with highest activities observed at pH 6.0 and 7.0. At pH 8.0 and 9.0, LdcI activity is virtually undetectable. Surprisingly, the activity of the LdcI enzyme was unaffected by the presence of RavA under any of the conditions tested even at higher concentrations of RavA and LdcI or under different incubation conditions (data not shown). The inclusion of ViaA protein in the assay also failed to produce any alteration in the activity of the LdcI enzyme (data not shown).

Furthermore, LdcI activity in whole cell extracts was also not affected by deletion of the *ravA* gene (Fig. 8*B*), in which the enzyme was induced by growth in unbuffered LB media containing excess glucose. The utilization of glucose as a carbon source results in the decrease in the pH of the media as cells ferment the glucose and produce lactic and acetic acids (65). The addition of purified RavA and nucleotides to the extract also did not affect LdcI activity (data not shown). The lack of effect of RavA on LdcI activity *in vivo* was further confirmed by comparing the ability of WT and Δ*ravA* cells to recover from a decrease in pH using the CadBA system by growing cells in special indicator media (Fig. 8*C*). This media contains excess glucose, bromocresol purple as a pH indicator, and lysine for use by the CadBA system. The change in the pH of the medium over time can be tracked by monitoring the change in the absorbance of the indicator at 590 nm. As shown in Fig. 8*C*, both WT

and Δ*ravA* cells experience an initial decrease in pH from 6.1 to ~5.0 but then recover, eventually raising the pH of the medium back to pH 6.1. On the other hand, a Δ*cadB* mutant, which is also deficient in LdcI/CadA production (data not shown), cannot restore the pH of the media, showing that pH recovery is dependent upon a functional CadBA system. Both WT and Δ*ravA* strains have equal recovery rates, showing that the lysine-dependent response to low pH does not appear to be compromised in the knock-out strain.

The ability of WT and Δ*ravA* cells to respond to a more extreme acid challenge was also examined. Cells were grown to stationary phase in LB media and then exposed to minimal media at pH 2.5, with and without added lysine, for 2 h. Cells were then diluted in LB media and plated on LB agar plates to measure cell viability (Fig. 8*D*). Both WT and Δ*ravA* cells appear to withstand this extreme acid stress equally well in the presence of lysine, providing further evidence that the CadBA system does not appear to be compromised in the *ravA* deletion strain. Finally, although LdcI is strongly induced when cells are shifted from neutral pH to pH 5.5, no such induction is observed for RavA (Fig. 8*E*). RavA is also not induced by shift to high pH media (data not shown). The induction of LdcI or its levels were also not affected in *ravA* deletion or overexpression strains (data not shown). All the data presented above seem to strongly suggest that the RavA·LdcI complex does not function to regulate LdcI activity, but, rather, the purpose of the complex is to regulate the activity of the RavA protein.

The effect of LdcI on RavA ATPase was measured. RavA ATPase activity was assessed using 1 mM ATP substrate in the presence of ViaA, LdcI, LdcC, and BSA (Fig. 8*F*). None of the added proteins appear to possess significant ATPase activity of their own (*columns 1–4*). The activity of 0.25 μM RavA alone is shown (*column 5*). Addition of 0.5 μM BSA or 0.5 μM LdcC did not have any significant effect on RavA ATPase activity (*columns 6* and *7*) consistent with the lack of binding of BSA or LdcC to RavA. Addition of 0.5 μM LdcI results in 1.4-fold stimulation of RavA ATPase (*column 8*). Increasing the concentration of LdcI did not result in further stimulation of RavA ATPase (data not shown). This observed increase in activity can be explained in several ways. One possibility is that RavA may exist in a more active form upon binding LdcI; alternatively, LdcI may help stimulate RavA hexamer formation in the presence of nucleotide by acting as a scaffold, with a concomitant increase in the overall ATPase activity of the population. Addition of ViaA results in a 1.9-fold stimulation of RavA ATPase activity (*column 9*). RavA activity in the presence of both 0.5 μM LdcI and 0.25 μM ViaA was stimulated by 2.4-fold (*column 10*). Because the fold stimulation obtained is not an average of 1.4 and 1.9, this might indicate the possible formation of a ternary complex of RavA·ViaA·LdcI. Alternatively, in the presence of LdcI and ViaA, RavA exists in a different conformation or oligomeric state than in the presence of LdcI or ViaA alone. It should be noted that the stimulations observed in the above experiments are reproducible with different preparations of proteins.

Based on the above data, our current speculation is that LdcI functions to regulate RavA and that the RavA·LdcI complex is formed under certain conditions to modulate RavA function. Although we have identified a putative regulator of RavA, efforts are currently underway to determine the exact role of RavA and ViaA in the cell and the substrates targeted by this AAA+ and VWA system.

DISCUSSION

RavA·ViaA Might Play a Role in Metal Insertion—Our analysis of RavA reveals that it is a member of a distinct subfamily of the MoxR AAA+ proteins whose function remains poorly characterized. We were able to divide the MoxR proteins into six subfamilies (Fig. 1*A*). Intriguingly, despite the distant relationship between members of the MoxR-proper and CGN subfamilies, there appears to be a remarkable similarity in the nature of their function. The parallels between the importance of the CGN family members NorQ/NirQ and CbbQ for the production/activation of nitric-oxide reductase and Rubisco, respectively, and the importance of MoxR for the production of active methanol dehydrogenase are striking. Even the GvpN protein, although not important for the biogenesis of an enzyme, appears to be crucial for the production of the large proteinaceous structure that comprises gas vesicles in certain cyanobacteria and halophilic archaea. Thus, it does not seem unreasonable to presume that RavA proteins, and indeed members of the other uncharacterized MoxR subfamilies, may play similar roles.

The co-occurrence of genes encoding proteins with VWA domains with MoxR AAA+ genes is also notable. We have demonstrated that RavA and its corresponding VWA protein, ViaA, comprise an operon (Fig. 4). This is consistent with results reported for the NorQ/NirQ and CbbQ proteins, whose genes are also part of an operon containing immediately adjacent VWA protein-encoding genes. These VWA domain-containing proteins were also shown to be important in the biogenesis of active nitric-oxide reductase and Rubisco. Although the exact role of ViaA is unclear, one possibility is that ViaA and RavA function in a role similar to that of the metal-chelatases, a family of AAA+ proteins to which the MoxR family has been shown to be closely related (2, 66). In these metal-chelatases, the AAA+ components work in conjunction with VWA proteins to mediate the insertion of Co^{+2} or Mg^{+2} into porphyrin rings as part of the synthesis of cobalamin or (bacterio)chlorophyll, respectively (47). In the case of Mg-chelatase, one of the subunits, BchD, actually contains an AAA+ and VWA domain fused together on a single polypeptide, the only example of such an arrangement known in bacteria and archaea (19). It is intriguing to speculate that RavA and ViaA may, therefore, play a role in metal insertion, a process that may be important in the activation of their substrate(s). Interestingly, both the nitric-oxide reductase for which NorQ/NirQ are important and the Rubisco for which CbbQ is important depend upon metal ions for their function. Efforts are currently underway to explore this possibility.

Possible Implications of LdcI Binding to RavA—The interaction of RavA with LdcI is interesting, however, its exact role is puzzling. RavA does not appear to exert any effect upon the activity of LdcI under a range of different *in vitro* conditions (Fig. 8*A*). In addition, cells in which the RavA gene has been disrupted display normal LdcI induction and activity and do not appear to be compromised in their response to a variety of acid stresses (Fig. 8, *B–D*). RavA levels are also not induced by acid, and the protein is present under growth conditions in which the LdcI enzyme is not present (Fig. 8*E*). The interaction of LdcI with RavA does result in an increase in RavA ATPase activity, however, suggesting that the complex is indeed functionally important. A further increase is observed in the presence of ViaA, suggesting ternary complex formation. The interaction also appears to be highly specific to LdcI, because RavA does not interact with the closely related LdcC protein. One possibility is that the complex formed between RavA and LdcI represents a means of regulating RavA activity in response to acid stress conditions. Thus RavA can be envisioned to carry out an independent function of some form, possibly helping to mediate the folding/assembly of particular enzyme complexes during stationary phase. Upon exposure to acid stress conditions, levels of LdcI increase dramatically, leading to the formation of the RavA·LdcI complex. This complex may represent a way of sequestering RavA protein from its natural substrates in response to acid stress. Alternatively, the complex may provide a means of maintaining RavA function under acid stress conditions, something more in

line with the observed stimulation of RavA activity. By acting as a "scaffold," LdcI may stabilize RavA oligomers under acid stress conditions. It is also possible that the complex formed may lead to a "gain of function," directing RavA toward entirely new substrate proteins via localization and/or conformational changes.

Implications of the RavA·LdcI Complex Structure—EM analysis has provided us with an exceptional view of both the LdcI enzyme alone and in complex with RavA. The structure of the LdcI particle, deduced from the presented electron microscopy data (Fig. 7, *A–C*), confirms the suggestion of Sabo *et al.* (55) that the LdcI oligomer is composed of five stable dimers. The characterization of LdcI in that work had indeed indicated that the protein was dimeric at pH 8.0 and at low ionic strength, whereas lowering of the pH to 7.0 and a concomitant increase in ionic strength favored an association of dimers into decamers. The dimer-decamer equilibrium was shown to be dependent on protein concentration. These observations explain some presence of dimers in our experimental conditions. It should be noted that, based on a visual analysis of individual side views, Sabo *et al.* (55), proposed the orientation of the dimer to be roughly perpendicular to the plane of the ring. On the contrary, our three-dimensional reconstruction unambiguously demonstrates a pronounced rotation of the monomer inside the dimeric building block of the LdcI double-toroid.

The cage-like structure of the imaged RavA·LdcI complex makes it tempting to speculate that it may provide a space in which another protein or proteins might be confined. Proteins held in such a position might then be subject to remodeling by the RavA oligomers. Such a complex could thus represent a novel chaperone structure assembled under acid stress conditions when levels of LdcI enzyme increase dramatically.

In summary, considerable information has been gathered on the RavA protein and its interaction with ViaA and LdcI. Its regulation by σ^S clearly suggests an importance of this protein in stationary phase and general stress responses. However, the substrate targets of RavA and the significance of its interaction with LdcI are currently under investigation.

Acknowledgments—We thank Usheer Kanjee, Asad Merchant, Bharat Sharma, and Philip Wong for contributing to different aspects of this project. J. S. and W. A. H. thank Dr. L. Aravind at the National Center for Biotechnology Information, National Institutes of Health, Bethesda, MD for his help with the bioinformatic analysis.

REFERENCES

1. Neuwald, A. F., Aravind, L., Spouge, J. L., and Koonin, E. V. (1999) *Genome Res.* **9,** 27–43
2. Iyer, L. M., Leipe, D. D., Koonin, E. V., and Aravind, L. (2004) *J. Struct. Biol.* **146,** 11–31
3. Kunau, W. H., Beyer, A., Franken, T., Gotte, K., Marzioch, M., Saidowsky, J., Skaletz-Rorowski, A., and Wiebel, F. F. (1993) *Biochimie* (*Paris*) **75,** 209–224
4. Patel, S., and Latterich, M. (1998) *Trends Cell Biol.* **8,** 65–71
5. Ogura, T., and Wilkinson, A. J. (2001) *Genes Cells* **6,** 575–597
6. Hanson, P. I., and Whiteheart, S. W. (2005) *Nat. Rev. Mol. Cell Biol.* **6,** 519–529
7. Beyer, A. (1997) *Protein Sci.* **6,** 2043–2058
8. Frickey, T., and Lupas, A. N. (2004) *J. Struct. Biol.* **146,** 2–10
9. Van Spanning, R. J., Wansell, C. W., De Boer, T., Hazelaar, M. J., Anazawa, H., Harms, N., Oltmann, L. F., and Stouthamer, A. H. (1991) *J. Bacteriol.* **173,** 6948–6961
10. Jungst, A., and Zumft, W. G. (1992) *FEBS Lett.* **314,** 308–314
11. de Boer, A. P., van der Oost, J., Reijnders, W. N., Westerhoff, H. V., Stouthamer, A. H., and van Spanning, R. J. (1996) *Eur. J. Biochem.* **242,** 592–600
12. Bartnikas, T. B., Tosques, I. E., Laratta, W. P., Shi, J., and Shapleigh, J. P. (1997) *J. Bacteriol.* **179,** 3534–3540
13. Hayashi, N. R., Arai, H., Kodama, T., and Igarashi, Y. (1997) *Biochem. Biophys. Res. Commun.* **241,** 565–569
14. Hayashi, N. R., Arai, H., Kodama, T., and Igarashi, Y. (1999) *Biochem. Biophys. Res. Commun.* **265,** 177–183
15. Englert, C., Wanner, G., and Pfeifer, F. (1992) *Mol. Microbiol.* **6,** 3543–3550
16. Offner, S., Wanner, G., and Pfeifer, F. (1996) *J. Bacteriol.* **178,** 2071–2078
17. Mlouka, A., Comte, K., Castets, A. M., Bouchier, C., and Tandeau de Marsac, N. (2004) *J. Bacteriol.* **186,** 2355–2365
18. DasSarma, S., Arora, P., Lin, F., Molinari, E., and Yin, L. R. (1994) *J. Bacteriol.* **176,** 7646–7652
19. Whittaker, C. A., and Hynes, R. O. (2002) *Mol. Biol. Cell* **13,** 3369–3387
20. Xiong, J. P., Stehle, T., Zhang, R., Joachimiak, A., Frech, M., Goodman, S. L., and Arnaout, M. A. (2002) *Science* **296,** 151–155
21. Kachlany, S. C., Planet, P. J., Bhattacharjee, M. K., Kollia, E., DeSalle, R., Fine, D. H., and Figurski, D. H. (2000) *J. Bacteriol.* **182,** 6169–6176
22. Katerov, V., Lindgren, P. E., Totolian, A. A., and Schalen, C. (2000) *Curr. Microbiol.* **40,** 149–156
23. Willows, R. D. (2003) *Nat. Prod. Rep.* **20,** 327–341
24. Tatusov, R. L., Fedorova, N. D., Jackson, J. D., Jacobs, A. R., Kiryutin, B., Koonin, E. V., Krylov, D. M., Mazumder, R., Mekhedov, S. L., Nikolskaya, A. N., Rao, B. S., Smirnov, S., Sverdlov, A. V., Vasudevan, S., Wolf, Y. I., Yin, J. J., and Natale, D. A. (2003) *BMC Bioinformatics* **4,** 41
25. Altschul, S. F., Gish, W., Miller, W., Myers, E. W., and Lipman, D. J. (1990) *J. Mol. Biol.* **215,** 403–410
26. Tatusov, R. L., Galperin, M. Y., Natale, D. A., and Koonin, E. V. (2000) *Nucleic Acids Res.* **28,** 33–36
27. Thompson, J. D., Higgins, D. G., and Gibson, T. J. (1994) *Nucleic Acids Res.* **22,** 4673–4680
28. Felsenstein, J. (1996) *Methods Enzymol.* **266,** 418–427
29. Veerassamy, S., Smith, A., and Tillier, E. R. (2003) *J. Comput. Biol.* **10,** 997–1010
30. Yu, D., Ellis, H. M., Lee, E. C., Jenkins, N. A., Copeland, N. G., and Court, D. L. (2000) *Proc. Natl. Acad. Sci. U. S. A.* **97,** 5978–5983
31. Datsenko, K. A., and Wanner, B. L. (2000) *Proc. Natl. Acad. Sci. U. S. A.* **97,** 6640–6645
32. Sternberg, N. L., and Maurer, R. (1991) *Methods Enzymol.* **204,** 18–43
33. Butland, G., Peregrin-Alvarez, J. M., Li, J., Yang, W., Yang, X., Canadien, V., Starostine, A., Richards, D., Beattie, B., Krogan, N., Davey, M., Parkinson, J., Greenblatt, J., and Emili, A. (2005) *Nature* **433,** 531–537
34. Zhang, R. G., Skarina, T., Katz, J. E., Beasley, S., Khachatryan, A., Vyas, S., Arrowsmith, C. H., Clarke, S., Edwards, A., Joachimiak, A., and Savchenko, A. (2001) *Structure* (*Camb*) **9,** 1095–1106
35. Lanzetta, P. A., Alvarez, L. J., Reinach, P. S., and Candia, O. A. (1979) *Anal. Biochem.* **100,** 95–97
36. Phan, A. P., Ngo, T. T., and Lenhoff, H. M. (1982) *Anal. Biochem.* **120,** 193–197
37. Iyer, R., Williams, C., and Miller, C. (2003) *J. Bacteriol.* **185,** 6556–6561
38. Chomczynski, P., and Sacchi, N. (1987) *Anal. Biochem.* **162,** 156–159
39. Lee, J. E., and Ahn, T. I. (2000) *Res. Microbiol.* **151,** 605–618
40. Lemire, B. D., and Weiner, J. H. (1986) *Methods Enzymol.* **126,** 377–386
41. Shevchenko, A., Wilm, M., Vorm, O., and Mann, M. (1996) *Anal Chem.* **68,** 850–858
42. Hegerl, R. (1996) *J. Struct. Biol.* **116,** 30–34
43. Hegerl, R., and Altbauer, A. (1982) *Ultramicroscopy* **9,** 109–116
44. Ludtke, S. J., Baldwin, P. R., and Chiu, W. (1999) *J. Struct. Biol.* **128,** 82–97
45. Heymann, J. B. (2001) *J. Struct. Biol.* **133,** 156–169
46. Baker, T. S., and Cheng, R. H. (1996) *J. Struct. Biol.* **116,** 120–130
47. Fodje, M. N., Hansson, A., Hansson, M., Olsen, J. G., Gough, S., Willows, R. D., and Al-Karadaghi, S. (2001) *J. Mol. Biol.* **311,** 111–122
48. Wheeler, D. L., Barrett, T., Benson, D. A., Bryant, S. H., Canese, K., Church, D. M., DiCuccio, M., Edgar, R., Federhen, S., Helmberg, W., Kenton, D. L., Khovayko, O., Lipman, D. J., Madden, T. L., Maglott, D. R., Ostell, J., Pontius, J. U., Pruitt, K. D., Schuler, G. D., Schriml, L. M., Sequeira, E., Sherry, S. T., Sirotkin, K., Starchenko, G., Suzek, T. O., Tatusov, R., Tatusova, T. A., Wagner, L., and Yaschenko, E. (2005) *Nucleic Acids Res.* **33,** (Database Issue) D39–D45
49. Yoo, S. J., Seol, J. H., Shin, D. H., Rohrwild, M., Kang, M. S., Tanaka, K., Goldberg, A. L., and Chung, C. H. (1996) *J. Biol. Chem.* **271,** 14035–14040
50. Austin, S., and Dixon, R. (1992) *EMBO J.* **11,** 2219–2228
51. Starkova, N. N., Koroleva, E. P., Rumsh, L. D., Ginodman, L. M., and Rotanova, T. V. (1998) *FEBS Lett.* **422,** 218–220
52. Blattner, F. R., Plunkett, G., 3rd, Bloch, C. A., Perna, N. T., Burland, V., Riley, M., Collado-Vides, J., Glasner, J. D., Rode, C. K., Mayhew, G. F., Gregor, J., Davis, N. W., Kirkpatrick, H. A., Goeden, M. A., Rose, D. J., Mau, B., and Shao, Y. (1997) *Science* **277,** 1453–1474
53. Weber, H., Polen, T., Heuveling, J., Wendisch, V. F., and Hengge, R. (2005) *J. Bacteriol.* **187,** 1591–1603
54. Rigaut, G., Shevchenko, A., Rutz, B., Wilm, M., Mann, M., and Seraphin, B. (1999) *Nat. Biotechnol.* **17,** 1030–1032
55. Sabo, D. L., Boeker, E. A., Byers, B., Waron, H., and Fischer, E. H. (1974) *Biochemistry* **13,** 662–670

56. Sabo, D. L., and Fischer, E. H. (1974) *Biochemistry* **13,** 670–676
57. Park, Y. K., Bearson, B., Bang, S. H., Bang, I. S., and Foster, J. W. (1996) *Mol. Microbiol.* **20,** 605–611
58. Merrell, D. S., and Camilli, A. (1999) *Mol. Microbiol.* **34,** 836–849
59. Soksawatmaekhin, W., Kuraishi, A., Sakata, K., Kashiwagi, K., and Igarashi, K. (2004) *Mol. Microbiol.* **51,** 1401–1412
60. Meng, S. Y., and Bennett, G. N. (1992) *J. Bacteriol.* **174,** 2659–2669
61. Watson, N., Dunyak, D. S., Rosey, E. L., Slonczewski, J. L., and Olson, E. R. (1992) *J. Bacteriol.* **174,** 530–540
62. Auger, E. A., and Bennett, G. N. (1989) *Arch. Microbiol.* **151,** 466–468
63. Kikuchi, Y., Kojima, H., Tanaka, T., Takatsuka, Y., and Kamio, Y. (1997) *J. Bacteriol.* **179,** 4486–4492
64. Lemonnier, M., and Lane, D. (1998) *Microbiology* **144,** 751–760
65. Clark, D. P. (1989) *FEMS Microbiol. Rev.* **5,** 223–234
66. Wolf, Y. I., Rogozin, I. B., Kondrashov, A. S., and Koonin, E. V. (2001) *Genome Res.* **11,** 356–372

Formation of a Distinctive Complex between the Inducible Bacterial Lysine Decarboxylase and a Novel AAA+ ATPase

Jamie Snider, Irina Gutsche, Michelle Lin, Sabulal Baby, Brian Cox, Gareth Butland, Jack Greenblatt, Andrew Emili and Walid A. Houry

J. Biol. Chem. 2006, 281:1532-1546.
doi: 10.1074/jbc.M511172200 originally published online November 21, 2005
